Evaluation of transverse shear stresses in layered beams/plates/shells via stress recovery accounting for various CUF-based theories

Evaluation of transverse shear stresses in layered beams/plates/shells via stress recovery accounting for various CUF-based theories

M. Petrolo[a]*, R. Augello[a]†, E. Carrera[a,b]‡, D. Scano§, A. Pagani[a]¶

[a]MUL2 Lab, Department of Mechanical and Aerospace Engineering, Politecnico di Torino, Corso Duca degli Abruzzi 24, 10129 Torino, Italy.

[b]Department of Mechanical Engineering, College of Engineering, Prince Mohammad Bin Fahd University P.O. Box 1664. Al Khobar 31952. Kingdom of Saudi Arabia

Abstract: *This paper exploits the stress recovery technique to evaluate the out-of-plane stress components in the static analysis of composite beams, plates and shells. This technique is implemented in the framework of the Carrera Unified Formulation, an approach allowing the implementation of the theories of structures in a compact way. This work uses Taylor, Legendre and Jacobi polynomials with equivalent single-layer and layer-wise approaches. The finite element method is applied to provide numerical solutions. Multi-layered beams, plates and shells subjected to different loading and boundary conditions are studied to validate and assess the proposed technique. The results are compared with those from the literature and show that the stress recovery technique provides reasonable accuracy for the shear stresses, even with lower-order models. Furthermore, results confirm that, when dealing with thick structures, the adoption of layer-wise models is mandatory to obtain accurate results.*

Keywords: Composite structures; Layer-Wise, Equivalent Single-Layer; Beam, plate, shell models; Taylor, Lagrange, Jacobi polynomials; Stress recovery.

1 Introduction

The accuracy of stress analysis is highly dependent on the theory adopted to solve the three-dimensional (3D) continuum problem for one-dimensional (1D) and two-dimensional (2D) structures. In particular, out-of-plane stress components are greatly affected by the chosen approximation. As an example, classical theories, such as the Euler-Bernoulli Beam Model

*Associate Professor. Corresponding author. Email: marco.petrolo@polito.it
†Assistant Professor. E-mail: riccardo.augello@polito.it
‡Full Professor. Email: erasmo.carrera@polito.it
§PhD Student. E-mail: daniele.scano@polito.it
¶Associate Professor. Email: alfonso.pagani@polito.it

(EBBM) [1] for 1D structures, or Kirchhoff-Love theory [2, 3] and Classical Lamination Theory (CLT) [4] for 2D metallic and composite structures, respectively, neglect the out-of-plane stresses. Improved classical theories were developed afterwards, for instance, the Timoshenko Beam Model (TBM) [5] for beams and First Shear Deformation Theory (FSDT), based on the works by Reissner [6] and Mindlin [7], for 2D structures. However, since the transverse shear stresses are considered constant via Hooke's law, the homogeneous conditions are violated at the top and bottom edges of the structure.

As far as layered composite structures are concerned, they show non-continuous mechanical material properties. The high values of Young's moduli orthotropic ratio - E_L/E_T and E_L/E_z with L as the fiber direction while T and z orthogonal to L - and the low transverse shear moduli ratio - G_{LT}/E_L and G_{TT}/E_L) - lead to higher transverse shear and normal stress deformability than isotropic cases. For accurate analyses, the Layer-Wise (LW) approach is often used due to the possibility of assigning sets of generalized degrees of freedom to each layer, see Carrera [8]. However, the LW technique may require a higher computational cost than the Equivalent Single Layer (ESL), in which the multilayered structure is modeled as a single layer with homogenized properties. ESL may lower the computational cost but could affect the result accuracy.

When dealing with 1D structures, improvements in classical models have been proposed to account for non-classical effects and non-conventional materials, as described in Novozhilov [9]. Extensive reviews for 1D theories can be found in Kapania and Raciti [10, 11] and Carrera *et al.* [12]. Warping functions to capture the deformations of the beam cross-section were proposed by Vlasov [13]. Ambrosini, Riera *et al.* [14], Mechab, Meiche et al. [15] and Friberg [16], adopted these functions for the analysis of thin-walled structures. Ganapathi *et al.* [17] proposed finite elements to study sandwich beams that account for transverse shear and warping. A family of finite elements considering a Heaviside function was developed by Vidal and Polit [18]. Moreover, Schardt [19] suggested the so-called Generalized Beam Theory, which expresses the displacement field as a linear combination of cross-sectional deformation modes. Another class of advanced 1D models is referred to as VABS [20] and has been developed using asymptotic methods.

Concerning 2D plate and shell theories, in addition to the already mentioned classical models, other theories have been implemented as shown in comprehensive reviews [21, 22]. Examples of higher-order theories with the ESL approach are those developed by Reddy [23], the so-called zig-zag theories firstly proposed by Murakami [24], and those based on Reissner's Mixed Variational Theorem (RMVT) developed by Carrera [25]. Furthermore, Rammerstorfer *et al.* [26], Reddy [27], Mawenya and Davies [28], and Noor and Burton [29] developed FE implementations using LW theories.

The reduction of accuracy of ESL models is particularly evident for the out-of-plane stress components when evaluated using Hooke's law, as it is commonly done. Alternatively, those stress components can be evaluated in a post-processing phase via the integration of the indefinite equilibrium equations of 3D elasticity [30]. This procedure is also known as the stress recovery technique, and it uses the first derivatives of the in-plane stresses integrated into the out-of-plane direction. Patni *et al.* [31] studied beams with the stress recovery method in the framework of Carrera Unified Formulation (CUF) using serendipity Lagrange expansion. When dealing with 2D structures, Carrera [22] compared Taylor-Like and Legendre expansions to study plates and shells with stress recovery technique. Finally, Park *et al.* [32] proposed a nonlinear predictor-corrector procedure for accurately recovering stresses in laminated plates.

The stress recovery technique is exploited in the present work to analyze composite beams,

plates, and shells. To evaluate the effect of the employed theory of structure on the out-of-plane stresses evaluated using Hooke's law and stress recovery, the Carrera Unified Formulation is exploited. CUF allows for using 1D beam and 2D plate and shell models of composite structures, and the approximation used, i.e., the theory of structure, is considered input of the analysis. This way, high- LW to low-order ESL models can be built without developing any *ad-hoc* theory. This paper implements three types of structural theories based on Taylor, Lagrange, and Jacobi polynomials in both ESL and LW ways.
This paper is structured as follows: Section 2 describes how the governing equations and the relative finite element arrays are evaluated for the unified models of beams, plates, and shells. Furthermore, the post-processing of the out-of-plane stress via the integration of the 3D indefinite equilibrium equations is presented in Section 3. Section 4 shows four benchmarks from the literature and the related results—finally, the main conclusions.

2 Governing equations for unified beam, plate and shell models

The composite beam, plate and shell models considered in this work are depicted in Fig. 1. The 1D beam model is considered in a Cartesian reference system, with the axis along the

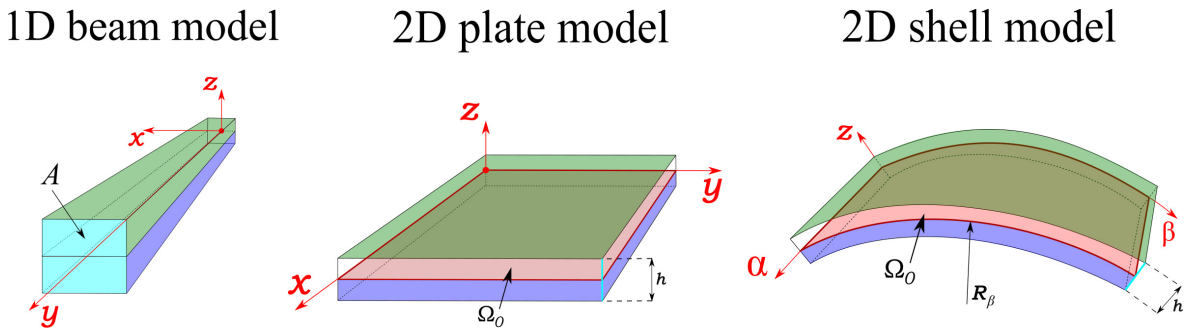

Figure 1: Beam, plate and shell composite structures. A Cartesian reference system is employed for the 1D beam and 2D plate models (x, y, z), whereas a curvilinear system (α, β, z) is considered for the 2D shell model.

y-direction, while the cross-section A is over the x, z plane. The same reference system is used for the 2D plate model, and the mid-surface Ω_0 lays on the x, y plane, whereas the z coordinate is used along the thickness direction. Finally, the shell uses a curvilinear reference frame (α, β, z), where α and β are the two in-plane directions and z is the thickness one. Single curvature shells, i.e. cylindrical shells, are considered in this work, with curvature radius R_β. The displacement vector is introduced as

$$\mathbf{u}^k(x,y,z) = \left\{ \begin{array}{ccc} u_x^k & u_y^k & u_z^k \end{array} \right\}^T, \quad \mathbf{u}^k(\alpha,\beta,z) = \left\{ \begin{array}{ccc} u_\alpha^k & u_\beta^k & u_z^k \end{array} \right\}^T \tag{1}$$

where k indicates the generic layer of the composite structure. The stress, $\boldsymbol{\sigma}^k$, and strain, $\boldsymbol{\epsilon}^k$, components are expressed in the vectorial form as follows:

$$\begin{aligned} \boldsymbol{\sigma}^k &= \left\{ \begin{array}{cccccc} \sigma_{xx}^k & \sigma_{yy}^k & \sigma_{zz}^k & \sigma_{xz}^k & \sigma_{yz}^k & \sigma_{xy}^k \end{array} \right\}^T, \quad \boldsymbol{\epsilon}^k = \left\{ \begin{array}{cccccc} \epsilon_{xx}^k & \epsilon_{yy}^k & \epsilon_{zz}^k & \epsilon_{xz}^k & \epsilon_{yz}^k & \epsilon_{xy}^k \end{array} \right\}^T \\ \boldsymbol{\sigma}^k &= \left\{ \begin{array}{cccccc} \sigma_{\alpha\alpha}^k & \sigma_{\beta\beta}^k & \sigma_{zz}^k & \sigma_{\alpha z}^k & \sigma_{\beta z}^k & \sigma_{\alpha\beta}^k \end{array} \right\}^T, \quad \boldsymbol{\epsilon}^k = \left\{ \begin{array}{cccccc} \epsilon_{\alpha\alpha}^k & \epsilon_{\beta\beta}^k & \epsilon_{zz}^k & \epsilon_{\alpha z}^k & \epsilon_{\beta z}^k & \epsilon_{\alpha\beta}^k \end{array} \right\}^T \end{aligned} \tag{2}$$

The displacement-strain relations are expressed as

$$\boldsymbol{\epsilon}^k = \mathbf{b}\mathbf{u}^k \tag{3}$$

where $\mathbf{b}$ is the matrix of differential operators [33, 34]).
Linear elastic orthotropic materials are considered in this work. Consequently, the constitutive relation using Hooke's law reads as:

$$\boldsymbol{\sigma}^k = \mathbf{C}^k\boldsymbol{\epsilon}^k, \tag{4}$$

where $\mathbf{C}^k$ is the material elastic matrix, whose explicit form can be found in [35, 36].
Within the framework of CUF, the 3D displacement field, $\mathbf{u}(x, y, z)$, of the 1D beam, 2D plate and $\mathbf{u}(\alpha, \beta, z)$ of shell models can be written as follows:

$$\mathbf{u}^k(x, y, z) = F^k_\tau \mathbf{u}^k_\tau, \qquad \delta\mathbf{u}^k(x, y, z) = F^k_s \delta\mathbf{u}^k_s \tag{5}$$

$$\tau = 1, 2, ..., M, \qquad s = 1, 2, ..., M \tag{6}$$

where F_τ and F_s are the expansion functions of the generalized displacements $\mathbf{u}^k_\tau$ and virtual variations $\delta\mathbf{u}^k_s$, respectively. The Einstein convention with the repeated indexes τ and s is assumed, M denotes the order of the expansion, and δ stands for the variation. This notation allows adopting any structural theories and selecting the desired degree of precision. Appendix A describes the adopted expansion functions, namely Taylor, Lagrange and Jacobi polynomials. The generalized displacements $\mathbf{u}^k_\tau$ and variations $\delta\mathbf{u}^k_s$ are discretized by means of the Finite Element Method (FEM). Thus, introducing FEM in Eq. (5), the following relations can be written

$$\mathbf{u}^k(x, y, z) = N_i F^k_\tau \mathbf{q}^k_{\tau i}, \qquad \delta\mathbf{u}^k(x, y, z) = N_j F^k_s \delta\mathbf{q}^k_{sj} \tag{7}$$

$$i = 1, 2, ..., N_n, \qquad j = 1, 2, ..., N_n \tag{8}$$

where N_i and N_j stand for the shape functions, the repeated subscripts i and j indicate summation, N_n is the number of the FE nodes per element, and $\mathbf{q}_{\tau i}$ and $\delta\mathbf{q}_{sj}$ are the vectors of the FE nodal parameters. The expansions of the 3D displacement field for beams, plates and shells are reported in Table 1. Well-known Lagrange-based shape functions, N_i and N_j,

Formulation	3D Field	FEM+CUF Expansions		
1D beam :	$\mathbf{u}^k(x, y, z)$	$N^k_i(y)$	$F^k_\tau(x, z)$	$\mathbf{q}^k_{\tau i}$
	$\delta\mathbf{u}^k_s(y)$	$N^k_j(y)$	$F^k_s(x, z)$	$\delta\mathbf{q}^k_{sj}$
2D plate :	$\mathbf{u}^k(x, y, z)$	$N^k_i(x, y)$	$F^k_\tau(z)$	$\mathbf{q}^k_{\tau i}$
	$\delta\mathbf{u}^k(x, y, z)$	$N^k_j(x, y)$	$F^k_s(z)$	$\delta\mathbf{q}^k_{sj}$
2D shell :	$\mathbf{u}^k(\alpha, \beta, z)$	$N^k_i(\alpha, \beta)$	$F^k_\tau(z)$	$\mathbf{q}^k_{\tau i}$
	$\delta\mathbf{u}^k(\alpha, \beta, z)$	$N^k_j(\alpha, \beta)$	$F^k_s(z)$	$\delta\mathbf{q}^k_{sj}$

Table 1: Overview of generalized primary unknowns. τ and s are repeated indexes with $\tau = 1, 2, ..., M$ and $s = 1, 2, ..., M$, while M denotes the order of expansion. i and j are repeated indexes with $i = 1, 2, ..., N_n$ and $j = 1, 2, ..., N_n$, where N_n is the number of the FE nodes per element.

are adopted [35]. In this work, one-dimensional FE with four nodes (B4) are adopted for beams, i.e., a cubic approximation along the y-axis is assumed. On the other hand, 2D nine-node bi-quadratic FE (Q9) are adopted as the shape functions for plates and shells.
The principle of virtual displacements is used to derive the governing equations,

$$\delta L_i = \int_{V_k} (\delta\boldsymbol{\epsilon}^T\boldsymbol{\sigma})\mathrm{d}V_k \quad = \quad \delta L_e \tag{9}$$

where V_k is the integration domain, δL_i is the variation of the internal work, and δL_e is the variation of the external work. Introducing the geometrical relations, Eq. (3), the constitutive equations, Eq. (4), CUF and FEM, Table 1, into Eq. (9), the following governing equations are obtained:

$$\delta \mathbf{q}^k_{sj} : \ \mathbf{k}^{kij\tau s} \, \mathbf{q}^k_{\tau i} = \mathbf{p}^k_{sj} \tag{10}$$

where $\mathbf{k}^{kij\tau s}$ is a 3×3 matrix, referred to as the fundamental nucleus of the mechanical stiffness matrix. The stiffness matrix of each layer k is obtained from the expansion of the fundamental nucleus on the indexes τ and s. $\mathbf{p}_{sj}$ is a 3×1 matrix, and is the fundamental nucleus of the external load. For the sake of brevity, $\mathbf{k}^{kij\tau s}$ and $\mathbf{p}_{sj}$ are not explicitly shown, but they can be found in [34, 37]. The assembly over all nodes and elements leads to

$$\mathbf{K} \, \mathbf{U} = \mathbf{P} \tag{11}$$

where $\mathbf{K}$, $\mathbf{U}$ and $\mathbf{P}$ are the stiffness matrix, the nodal displacements and the nodal forces of the structure, respectively.

3 A posteriori evaluation of out-of-plane stress components

As previously described, Hooke's law, Eq. (4), allows for the evaluation of the in-plane and out-of-plane stress components using strains and, in the case of low-order theories, the accuracy of stress components from Hooke's law may be unsatisfactory. This is especially true for the out-of-plane components of the stress vector. To overcome this issue, those components can be evaluated using a post-processing procedure via the integration of the 3D indefinite equilibrium equations, i.e., a stress recovery technique, and using the in-plane stress components calculated with Hooke's law. Such a technique guarantees that the homogeneous conditions at the top and bottom edges of the structure and the continuity of shear stresses at the layer interfaces are fulfilled. Fig. 2 illustrates the integration direction for 1D beam and 2D plate and shell formulations. The indefinite equilibrium equations of 3D elasticity for 1D beam and 2D plate formulations are

$$\begin{cases} \delta u_x : & \sigma_{xx,x} + \sigma_{xz,z} + \sigma_{xy,y} = g_x \\ \delta u_y : & \sigma_{yx,x} + \sigma_{yz,z} + \sigma_{yy,y} = g_y \end{cases} \tag{12}$$

Furthermore, the volume forces are imposed as follows

$$\boldsymbol{g} = \left\{ \begin{array}{ccc} g_x & g_y & g_z \end{array} \right\}^T = \left\{ \begin{array}{ccc} 0 & 0 & 0 \end{array} \right\}^T \tag{13}$$

Integrating from z^{i-1} to z^i, see Fig. 2,

$$\begin{cases} \sigma^i_{xz} = & \sigma^{i-1}_{xz} - \int_{i-1}^{i} \left(\sigma_{xx,x} + \sigma_{xy,y} \right) dz \\ \sigma^i_{yz} = & \sigma^{i-1}_{yz} - \int_{i-1}^{i} \left(\sigma_{yy,y} + \sigma_{xy,x} \right) dz \end{cases} \tag{14}$$

For shells, the indefinite equilibrium equations are written as follows

$$\begin{cases} \delta u_x : & \frac{\partial \sigma_{\alpha z}}{\partial z} + \sigma_{\alpha z} \left(\frac{2}{R_\alpha \, H_\alpha} + \frac{1}{R_\beta \, H_\beta} \right) + \frac{1}{H_\alpha} \frac{\partial \sigma_{\alpha\alpha}}{\partial \alpha} + \frac{1}{H_\beta} \frac{\partial \sigma_{\alpha\beta}}{\partial \beta} = g_\alpha \\ \\ \delta u_y : & \frac{\partial \sigma_{\beta z}}{\partial z} + \sigma_{\beta z} \left(\frac{1}{R_\alpha \, H_\alpha} + \frac{2}{R_\beta \, H_\beta} \right) + \frac{1}{H_\beta} \frac{\partial \sigma_{\beta\beta}}{\partial \beta} + \frac{1}{H_\alpha} \frac{\partial \sigma_{\alpha\beta}}{\partial \alpha} = g_\beta \end{cases} \tag{15}$$

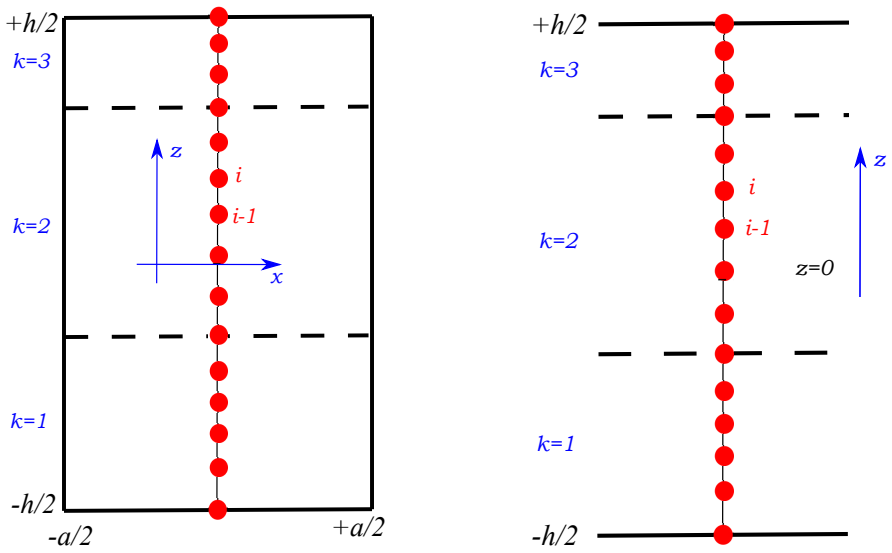

Figure 2: Integration of 3D equilibrium equations for 1D beam (a) and 2D plate and shell (b) formulations.

with

$$\begin{cases} H_\alpha = & 1 + \frac{z}{R_\alpha} \\ \\ H_\beta = & 1 + \frac{z}{R_\beta} \end{cases} \tag{16}$$

Furthermore, the volume forces are imposed as follows

$$\boldsymbol{g} = \left\{ \begin{array}{ccc} g_\alpha & g_\beta & g_z \end{array} \right\}^T = \left\{ \begin{array}{ccc} 0 & 0 & 0 \end{array} \right\}^T \tag{17}$$

In this paper, only cylindrical shells are considered and the equations are modified as follows

$$\begin{cases} \delta u: & \frac{\partial \sigma_{\alpha z}}{\partial z} + \sigma_{\alpha z} \left(\frac{1}{R_\beta \, H_\beta} \right) = -\frac{\partial \sigma_{\alpha\alpha}}{\partial \alpha} - \frac{1}{H_\beta} \frac{\partial \sigma_{\alpha\beta}}{\partial \beta} \\ \\ \delta v: & \frac{\partial \sigma_{\beta z}}{\partial z} + \sigma_{\beta z} \left(\frac{2}{R_\beta \, H_\beta} \right) = -\frac{1}{H_\beta} \frac{\partial \sigma_{\beta\beta}}{\partial \beta} - \frac{\partial \sigma_{\alpha\beta}}{\partial \alpha} \end{cases} \tag{18}$$

with

$$\begin{cases} H_\alpha = & 1 \\ \\ H_\beta = & 1 + \frac{z}{R_\beta} \end{cases} \tag{19}$$

Eq. (18) is solved using the trapezoidal rule, i.e.,

$$\begin{cases} \sigma^i_{\alpha z} = \left(\frac{\sigma^{i-1}_{\alpha z} (1 - (z^i - z^{i-1}))}{H_\beta R_\beta} + \int_{i-1}^{i} \left(-\frac{\partial \sigma_{\alpha\alpha}}{\partial \alpha} - \frac{1}{H_\beta} \frac{\partial \sigma_{\alpha\beta}}{\partial \beta} \right) dz \right) / \left(\frac{1 + (z^i - z^{i-1})}{H_\beta R_\beta} \right) \\ \\ \sigma^i_{\beta z} = \left(\frac{\sigma^{i-1}_{\beta z} (1 - (z^i - z^{i-1}))}{H_\beta R_\beta} + \int_{i-1}^{i} \left(-\frac{1}{H_\beta} \frac{\partial \sigma_{\beta\beta}}{\partial \beta} - \frac{\partial \sigma_{\alpha\beta}}{\partial \alpha} \right) dz \right) / \left(\frac{1 + (z^i - z^{i-1})}{H_\beta R_\beta} \right) \end{cases} \tag{20}$$

B1: Two-layer beam [38]	B2: Three-layer plate [39]
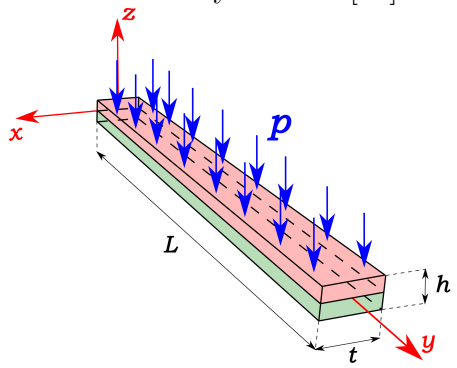	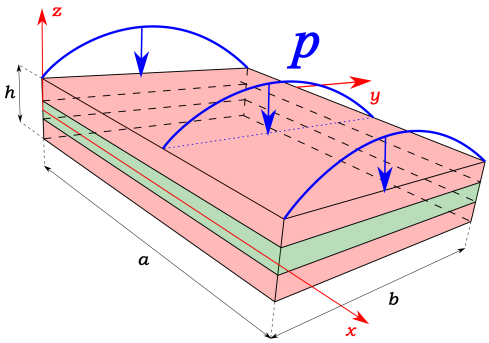
$L/h = 20$ and $h/t = 0.5$ Cantilever beam with uniform pressure on top, $p = 1000$Pa	$b/h = 4, 100$ and $a/b = 1$ Simply-supported, with a transverse sinusoidal pressure $p = p_z \sin(\frac{\pi y}{b})$ on top, $p_z = 1$Pa
B3: Five-layer sandwich plate [40, 41]	B4: Three-layer shell [42, 25]
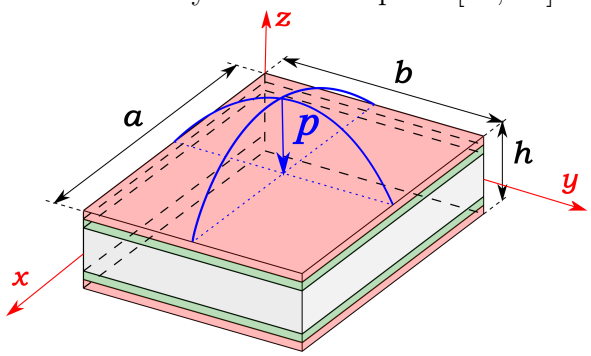	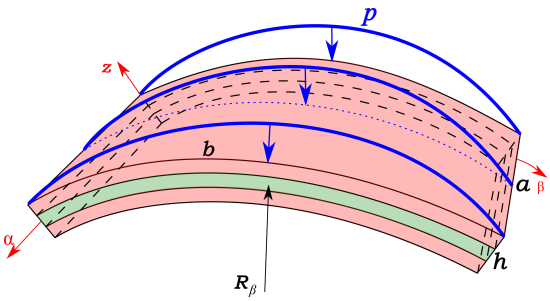
$a/h = 100$, $a = b$, $h_{\text{core}} = 8mm$, $h_{\text{skin}} = 0.5mm$ Simply-supported with a transverse sinusoidal pressure $p = p_z \sin(\frac{\pi x}{a})\sin(\frac{\pi y}{b})$ on top , $p_z = 1$Pa	$R_\beta/b = \pi/3$, $R_\beta/h = 4, 100$ and $a = 1$ Simply-supported with a transverse sinusoidal pressure $p = p_z \sin(\frac{\pi \beta}{b})$ on top, $p_z = 1$Pa

Table 2: Geometrical and loading conditions of the four benchmarks.

4 Numerical results

In this section, four benchmarks from the literature are considered to verify the stress recovery technique, and they are described in Table 2. In particular, the shear stresses are evaluated by using Hooke's law and the stress recovery method, and compared with reference solutions. Table 3 shows the system for labelling the adopted theory. TP indicates Taylor with order P, ELN stands for equivalent single-layer Lagrange and LLN is layer-wise Lagrange with N number of points used in the domain, and LJP indicates layer-wise Jacobi of $P-th$ polynomial order, whereas EJP stands for equivalent single-layer Jacobi. For examples,

- LL5: LW, five points Lagrange (Fourth-order).
- EJ5: ESL, Jacobi (Fifth-order).

For the shear stresses results, H indicates the use of Hooke's law, and I stands for the stress recovery method.

Approach	*Taylor*	*Lagrange*	*Jacobi*
ESL	TP	ELN	EJP
LW	-	LLN	LJP

Table 3: Theories adopted in the present work. N is the number of points used for each section element and P is the polynomial order.

4.1 Two-layer beam

A two-layer is studied as the first case. and retrieved from [38]. The same beam is considered in two different cases, composite and bi-metallic. In the former, the material properties are $E_L/E_T = 25$, $E_T = E_3$, $\nu_{LT} = \nu_{T3} = \nu_{L3} = 0.25$, $G_{LT}/E_T = 0.5$, $G_{L3}/E_T = G_{T3}/E_T = 0.2$, being L and T the longitudinal and transverse direction, respectively, and with the stacking sequence $[0°/90°]$. Concerning the bimetallic structure, the considered material properties are $E_1 = 210$ GPa, $\nu_1 = 0.3$, $E_2 = 75$ GPa and $\nu_1 = 0.3$, where 1 and 2 indicate the two layers of the beam. According to the LW approach, Lagrange and Jacobi models are developed by dividing the cross-section into two sub-domains, one per layer, in both cases.
Table 4 compares several ESL and LW kinematic models for the composite beam case. The values of transverse displacements, in-plane and shear stresses are shown. Furthermore, the number of degrees of freedom (DOF) is illustrated for comparison purposes. The related shear stress distributions are depicted in Figs. 3 and 4, by using Hooke's law and the stress recovery method, respectively.
Concerning the bimetallic structure, the results for transverse displacements, in-plane and shear stresses are shown in Table 5. On the other hand, Figs. 5 and 6 illustrate the shear stresses via Hooke's law and the stress recovery method, respectively.
Some remarks can be drawn from these results:

- In both cases, transverse displacements and in-plane stresses are accurately evaluated by LW and higher-order ESL models. EBBM and the other less-refined models, i.e., T1, EJ1 and EL4, cannot match the reference solution, according to Tables 4 and 5.
- Table 4 and Fig. 3 show that LW higher-order theories are needed when shear stresses are calculated through Hooke's Law. ESL models cannot describe the distribution, even if higher-order theories are adopted, unless the stress recovery is adopted.
- When shear stresses are evaluated for the bimetallic beam case, similar conclusions as for the composite beam case can be drawn. However, for this case, E_3 is different along the z direction and, such a transverse anisotropy, makes LW mandatory.

4.2 Three-layer composite plate

As a second case, a three-layer composite plate is studied. Both thick ($b/h = 4$) and thin ($b/h = 100$) configurations are considered. The study case was originally proposed by Pagano [39] and further investigated by Reddy [23]. An orthotropic material is employed with the following properties: $E_L/E_T = 25$, $E_T = E_3 = 1$, $\nu_{LT} = \nu_{T3} = \nu_{L3} = 0.25$, $G_{LT}/E_T = G_{L3}/E_T = 0.5$, $G_{T3}/E_T = 0.2$. The stacking sequence is $[90°/0°/90°]$. The results of transverse displacements, in-plane and shear stresses are reported in the following non-dimensional form:

$$\overline{u}_z = \frac{100\ E_T\ u_z}{\left(\frac{b}{h}\right)^4\ h\ p_z} \qquad \overline{\sigma}_{xx} = \frac{\sigma_{xx}}{\left(\frac{b}{h}\right)^2\ p_z} \qquad \overline{\sigma}_{xz} = \frac{\sigma_{xz}}{\left(\frac{b}{h}\right)\ p_z} \tag{21}$$

Model	$-u_z \times 10^3 mm$	$\sigma_{yy} \times 10^3 MPa$	$\sigma_{yz} \times 10^3 MPa$		DOF
			H	I	
Taylor and Classical Models					
EBBM	5.140	92.96	—	23.14	198
TBM	5.265	92.38	10.07	23.20	198
T1	5.265	92.32	10.07	23.20	198
T3	5.240	91.61	15.45	23.04	660
T5	5.261	90.08	22.27	23.02	1386
T7	5.262	90.61	23.63	23.02	2376
LW Lagrange					
LL4	5.220	92.65	16.38	22.98	396
LL9	5.247	90.93	16.35	23.03	990
LL16[38]	5.263	90.33	23.00	23.04	1848
ESL Lagrange					
EL4	5.131	95.91	10.07	22.87	264
EL9	5.233	91.35	14.76	23.04	594
EL16	5.240	91.43	15.44	23.05	1056
LW Jacobi					
LJ1	5.220	92.65	16.38	22.98	396
LJ2	5.246	91.04	16.35	23.03	858
LJ3	5.263	90.40	23.04	23.04	1320
LJ4	5.263	90.27	23.02	23.01	1914
LJ5	5.263	90.30	23.01	23.01	2640
ESL Jacobi					
EJ1	5.131	95.91	10.07	22.87	264
EJ2	5.233	91.04	14.77	23.04	528
EJ3	5.240	91.55	15.44	23.03	792
EJ4	5.256	90.60	20.34	23.00	1122
EJ5	5.260	90.13	22.27	23.01	1518

Table 4: Transverse displacement and shear stresses of cantilever composite beam loaded by a uniform pressure with 1D formulation. u_z calculated in $[0, L, 0]$, σ_{yy} calculated in $[0, L/2, 0.05m]$ and σ_{yz} calculated in $[0, L/2, -0.025m]$.

Model	$-u_z \times 10^3 mm$	$\sigma_{yy} \times 10^3 MPa$	$\sigma_{yz} \times 10^3 MPa$		DOF
			H	I	
Taylor and Classical Models					
EBBM	0.2025	234.4	—	14.72	549
TBM	0.2029	234.8	14.80	15.45	549
T1	0.2029	234.8	14.80	14.94	549
T3	0.2006	234.9	15.49	13.25	1830
T5	0.2008	234.7	13.73	11.94	3843
T7	0.2009	234.8	12.37	12.24	6588
LW Lagrange					
LL4	0.2008	237.5	12.16	14.84	1098
LL9	0.2007	234.7	11.22	13.85	2745
LL16[38]	0.2008	234.8	11.58	13.87	5124
ESL Lagrange					
LL4	0.1629	234.8	14.79	14.59	732
LL9	0.2006	234.9	11.54	13.71	1647
LL16	0.2008	234.7	14.72	13.87	2928
LW Jacobi					
LJ1	0.2008	237.5	12.16	14.84	1098
LJ2	0.2008	234.7	11.74	13.68	2379
LJ3	0.2009	234.7	12.22	13.68	3660
LJ4	0.2010	234.9	13.09	12.41	5307
LJ5	0.2010	234.8	12.95	12.18	7320
ESL Jacobi					
EJ1	0.1629	234.8	14.79	14.59	732
EJ2	0.2006	235.0	11.35	13.68	1464
EJ3	0.2008	234.7	15.49	13.70	2196
EJ4	0.2009	234.8	15.64	12.19	3111
EJ5	0.2010	234.9	13.73	12.07	4209

Table 5: Transverse displacement and shear stresses of cantilever bimetallic beam loaded by a uniform pressure with 1D formulation. u_z calculated in $[0, L, 0]$, σ_{yy} calculated in $[0, L/2, -0.01249m]$ and σ_{yz} calculated in $[0, L/2, -0.01249m]$.

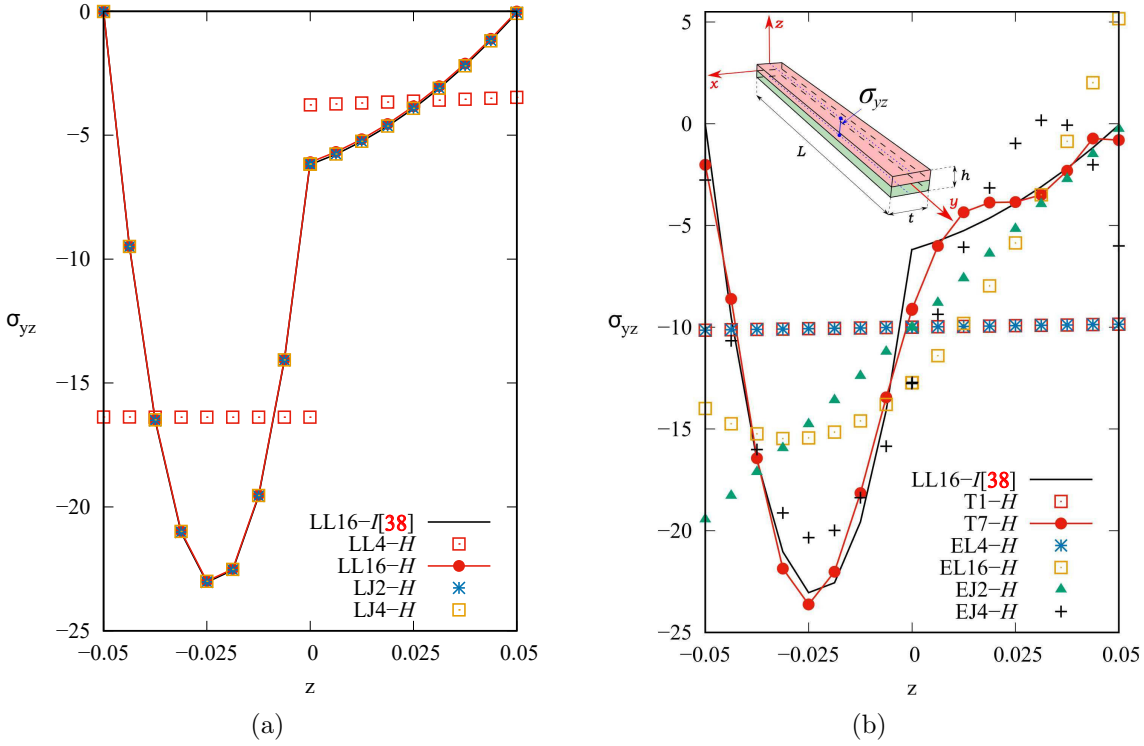

Figure 3: Shear stress in $[0, L/2, z]$ of cantilever two-layer composite beam loaded by a uniform pressure with 1D formulation using Hooke's law for LW (a) and ESL (b) approaches.

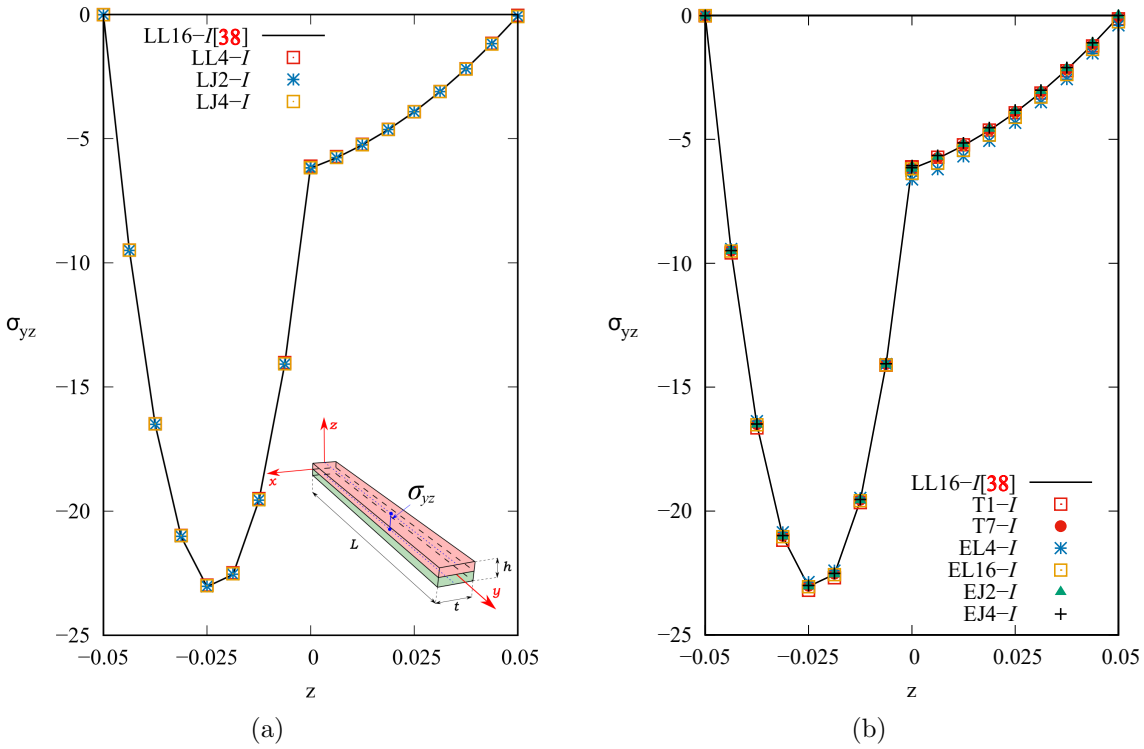

Figure 4: Shear stress in $[0, L/2, z]$ of cantilever two-layer composite beam loaded by a uniform pressure with 1D formulation using stress recovery for LW (a) and ESL (b) approaches.

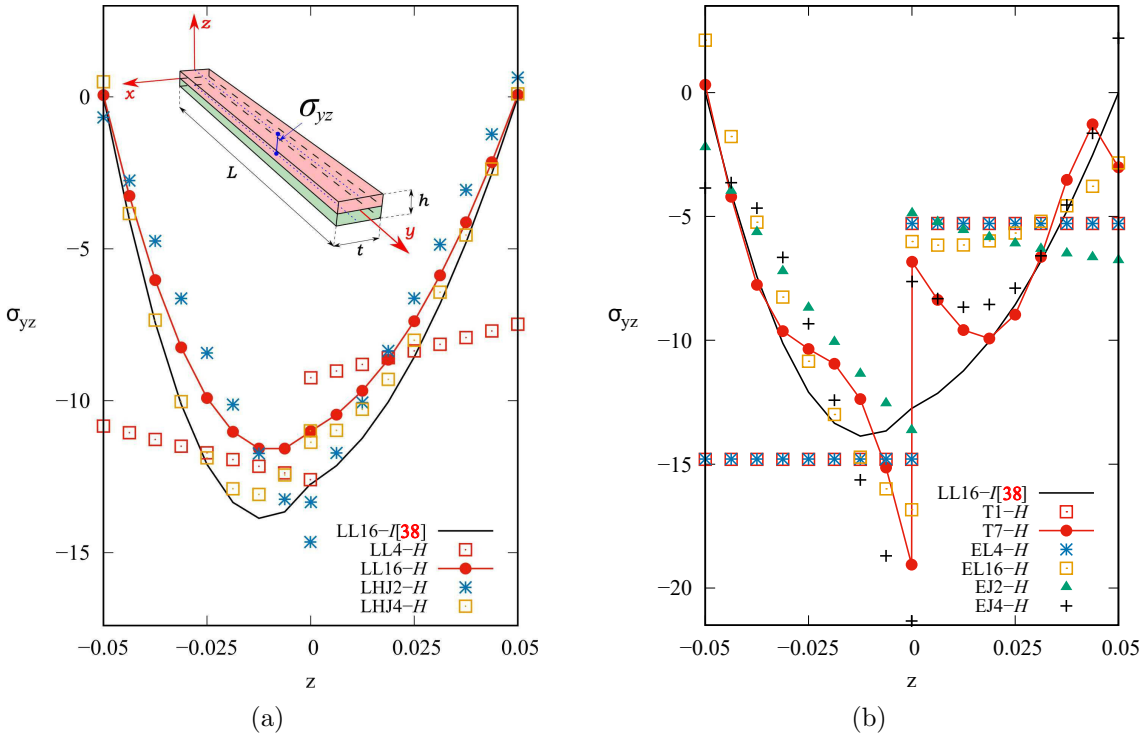

Figure 5: Shear stress in $[0, L/2, z]$ of cantilever bimetallic beam loaded by a uniform pressure with 1D formulation using Hooke's law for LW (a) and ESL (b) approaches for LW (a) and ESL (b) approaches.

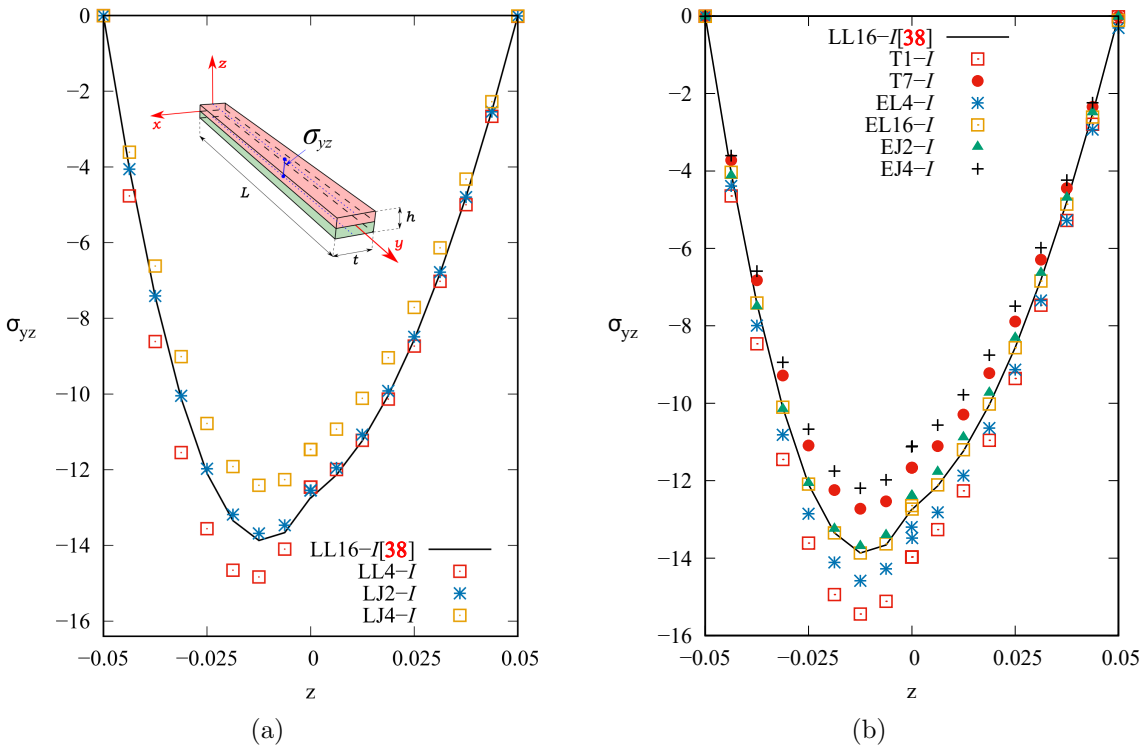

Figure 6: Shear stress in $[0, L/2, z]$ of cantilever bimetallic beam loaded by a uniform pressure with 1D formulation using stress recovery for LW (a) and ESL (b) approaches.

One sub-domain for each layer is used when adopting the LW Lagrange and Jacobi models. For the thin plate, the results are compared with the reference solution [23]. A preliminary convergence analysis is carried out, and the results are shown in Fig. 7 for the shear stresses using Hooke's law and the stress recovery method. It is carried out by adopting the LJ5 kinematics. In Table 6, the transverse displacements and the in-plane and shear stresses calculated by ESL and LW models are shown, and the related distributions of the shear stresses using Hooke's law are plotted in Fig. 8, while Fig. 9 illustrates the behaviour of the shear stresses via the stress recovery technique.
Regarding the thick plate, the results are compared with the exact solution provided by Pagano [39]. Table 6 reports results for the transverse displacements, in-plane and shear stresses as well as DOFs. The distributions of the shear stresses using Hooke's law and the stress recovery technique are reported in Figs. 10 and 11, respectively. The following considerations can be made:

- Regarding the displacements and the in-plane stresses for the thin plate, all the kinematic models can approximate them accurately. However, when the thick plate is taken into account, classical and lower-order ESL models cannot obtain reliable results. Same conclusions can be given for in-plane stresses.

- Considering the shear stresses calculated via Hooke's law for the thin case, only the LW with higher-order polynomials can almost fulfill the inter-laminar continuity and zero conditions at the top and bottom positions. The ESL theories are far from the reference solution, even for higher-order theories. This is more evident for the thick plate.

- If the stress recovery method is employed, this technique can improve the results for the LW models and the lower-order theories. In particular, when this strategy is applied to the thin plate, each kinematics matches the reference solution.

- Given a polynomial order, Taylor, ESL Lagrange and ESL Jacobi lead to the same results. This is also valid for LW Lagrange and Jacobi.

4.3 Five-layer composite sandwich plate

The third benchmark considers a thin sandwich plate ($a/h = 100$) from [40, 41]. The material properties are $E_L = 50$ GPa, $E_3 = E_T = 10$ GPa, $G_{LT} = G_{L3} = G_{T3} = 5$ GPa, $\nu_{LT} = \nu_{L3} = \nu_{Tz} = 0.25$ for the skins. The ply sequences of the bottom and top skins are $[0°/90°]$ and $[90°/0°]$, respectively. The properties of the material of the core are $E_L = E_T = 0.01$ MPa, $E_3 = 75.85$ MPa, $G_{LT} = G_{L3} = G_{T3} = 22.5$ MPa, $\nu_{LT} = \nu_{L3} = \nu_{T3} = 0.25$. When Lagrange and Jacobi models LW are used, five sub-domains are used along the thickness direction, one per layer.
A comparison for several kinematic models is listed in Table 7. Transverse displacements, in-plane and shear stresses are shown. Figs. 12 and 13 show the distributions for the shear stresses using Hooke's law and stress recovery method, respectively.
The following considerations can be drawn:

- Classical and lower-order ESL models cannot accurately evaluate the transverse displacements and the in-plane stresses; only higher-order kinematics such as T9, EL7 and EJ5 can catch the transverse displacements. On the other hand, LW theories are close to the reference solution.

Model	$b/h=4$					$b/h=100$				
	$\overline{u}_z$	$\overline{\sigma}_{xx}$	$\overline{\sigma}_{xz}$ (H)	$\overline{\sigma}_{xz}$ (I)	DOF	$\overline{u}_z$	$\overline{\sigma}_{xx}$	$\overline{\sigma}_{xz}$ (H)	$\overline{\sigma}_{xz}$ (I)	DOF
Exact[39]	2.887	1.176	—	0.358	—	—	—	—	—	—
Exact[23]	—	—	—	—	—	0.513	0.631	—	0.442	—
Taylor and Classical Models										
CLT	0.511	0.629	—	0.412	1302	0.510	0.630	—	0.288	9018
FSDT	2.093	0.633	0.160	0.441	1302	0.512	0.633	0.160	0.443	9018
T1	2.092	0.626	0.160	0.439	1302	0.512	0.633	0.160	0.443	9018
T3	2.687	1.136	0.285	0.380	2604	0.513	0.631	0.316	0.441	18036
T5	2.741	1.134	0.326	0.365	3906	0.514	0.631	0.402	0.441	27054
T7	2.807	1.152	0.374	0.359	5208	0.514	0.631	0.466	0.441	36072
T9	2.825	1.155	0.401	0.359	6510	0.514	0.631	0.494	0.441	45090
LW Lagrange										
LL2	2.864	1.003	0.361	0.358	2604	0.514	0.631	0.442	0.441	18036
LL3	2.881	1.155	0.355	0.353	4557	0.514	0.631	0.442	0.441	31563
LL4	2.887	1.173	0.359	0.358	6510	0.514	0.631	0.442	0.441	45090
LL5	2.887	1.173	0.359	0.358	8463	0.514	0.631	0.442	0.441	58617
LL6	2.887	1.173	0.359	0.358	9765	0.514	0.631	0.442	0.441	72144
LL7	2.887	1.173	0.359	0.358	12369	0.514	0.631	0.442	0.441	85671
ESL Lagrange										
EL2	2.092	0.626	0.160	0.439	1302	0.510	0.630	0.160	0.443	9018
EL3	2.074	0.651	0.159	0.439	1953	0.512	0.630	0.160	0.441	13527
EL4	2.687	1.136	0.285	0.380	2604	0.514	0.631	0.316	0.441	18036
EL5	2.685	1.134	0.285	0.380	3255	0.514	0.631	0.316	0.441	22545
EL6	2.741	1.134	0.374	0.365	3906	0.514	0.631	0.386	0.441	27054
EL7	2.741	1.134	0.374	0.365	4557	0.514	0.631	0.386	0.441	31563
LW Jacobi										
LJ1	2.864	1.003	0.361	0.358	2604	0.514	0.631	0.442	0.443	18036
LJ2	2.881	1.155	0.355	0.353	4557	0.514	0.631	0.442	0.441	31563
LJ3	2.887	1.173	0.359	0.358	6510	0.514	0.631	0.442	0.441	45090
LJ4	2.887	1.173	0.359	0.358	8463	0.514	0.631	0.442	0.441	58617
LJ5	2.887	1.173	0.359	0.358	9765	0.514	0.631	0.442	0.441	72144
ESL Jacobi										
EJ1	2.092	0.626	0.160	0.439	1302	0.510	0.630	0.160	0.441	9018
EJ2	2.074	0.651	0.159	0.439	1953	0.512	0.630	0.160	0.441	13527
EJ3	2.687	1.136	0.285	0.380	2604	0.514	0.631	0.316	0.441	18036
EJ4	2.685	1.134	0.285	0.380	3255	0.514	0.631	0.316	0.441	22545
EJ5	2.741	1.134	0.374	0.365	3906	0.514	0.631	0.386	0.441	27054

Table 6: Transverse displacement, in-plane and shear stresses of three-layer composite plate loaded by sinusoidal pressure with 2D formulation. $\overline{u}_z$ calculated in $[a/2, b/2, 0]$, $\overline{\sigma}_{xx}$ calculated in $[a/2, b/2, h/2]$, $\overline{\sigma}_{xz}$ calculated in $[a/2, 0, 0]$.

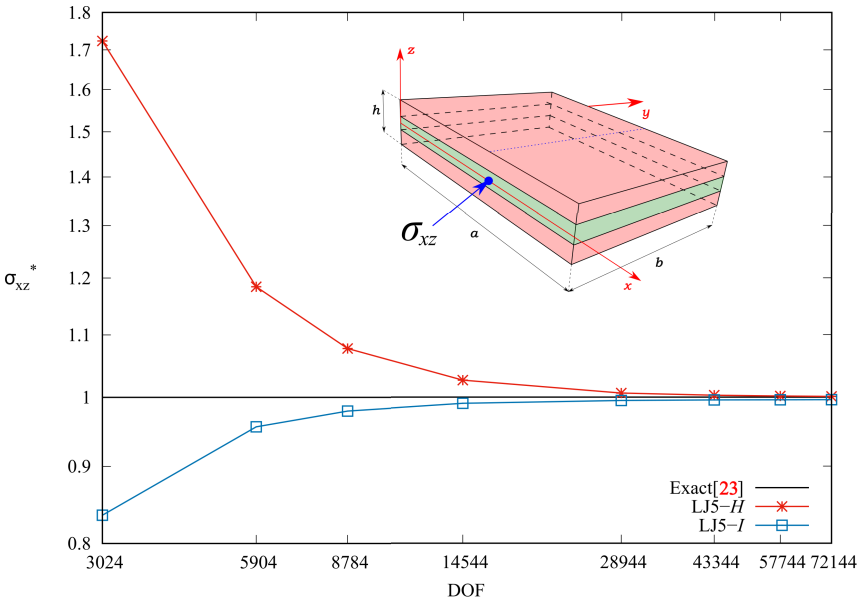

Figure 7: Convergence of shear stresses $\sigma^*_{xz} = \frac{\bar{\sigma}_{xz}}{\bar{\sigma}_{xz}(\text{Exact}[23])}$ in $[a/2, 0, 0]$ for three-layer composite plate loaded by sinusoidal pressure with 2D formulation for $b/h = 100$ case using Hooke's law and stress recovery technique.

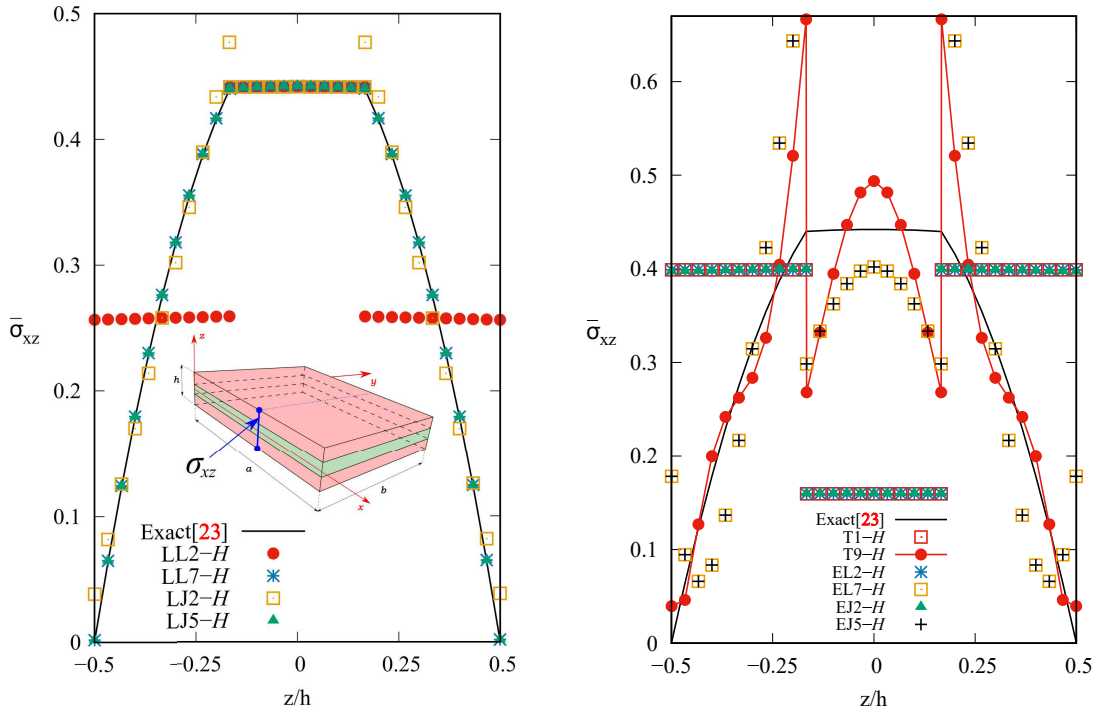

Figure 8: Shear stresses in $[a/2, 0, z]$ for three-layer composite plate loaded by sinusoidal pressure with 2D formulation for $b/h = 100$ case using Hooke's law for LW (a) and ESL (b) approaches.

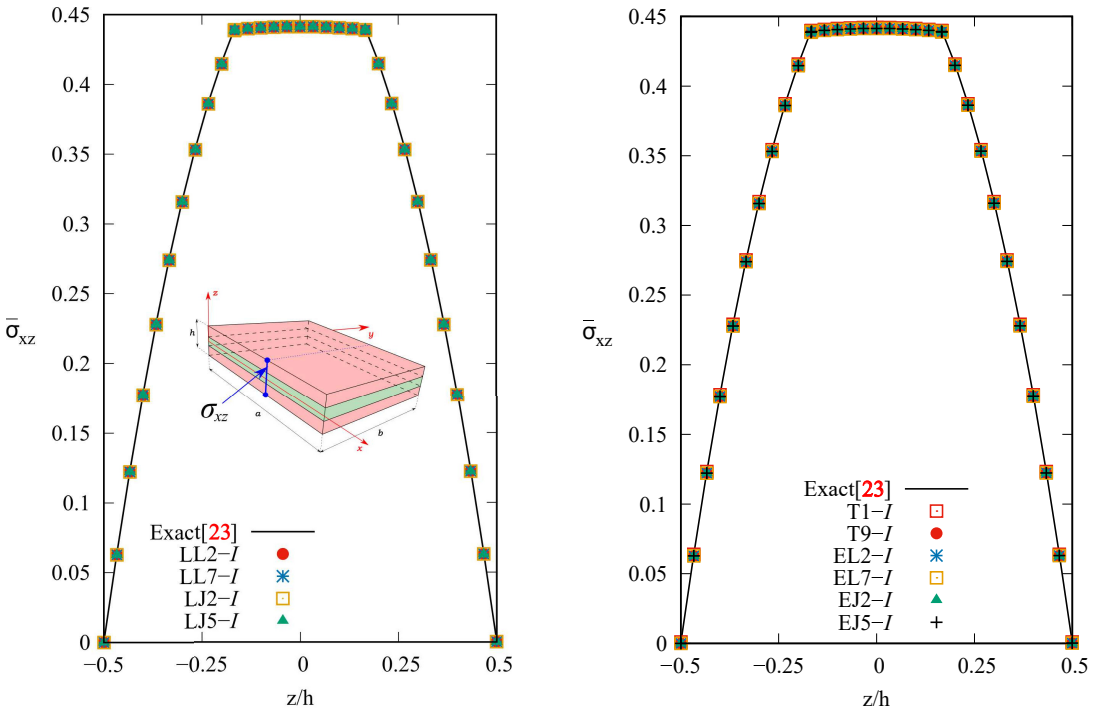

Figure 9: Shear stresses in $[a/2, 0, z]$ for three-layer composite plate with loaded by sinusoidal pressure with 2D formulation for $b/h = 100$ case using stress recovery for LW (a) and ESL (b) approaches.

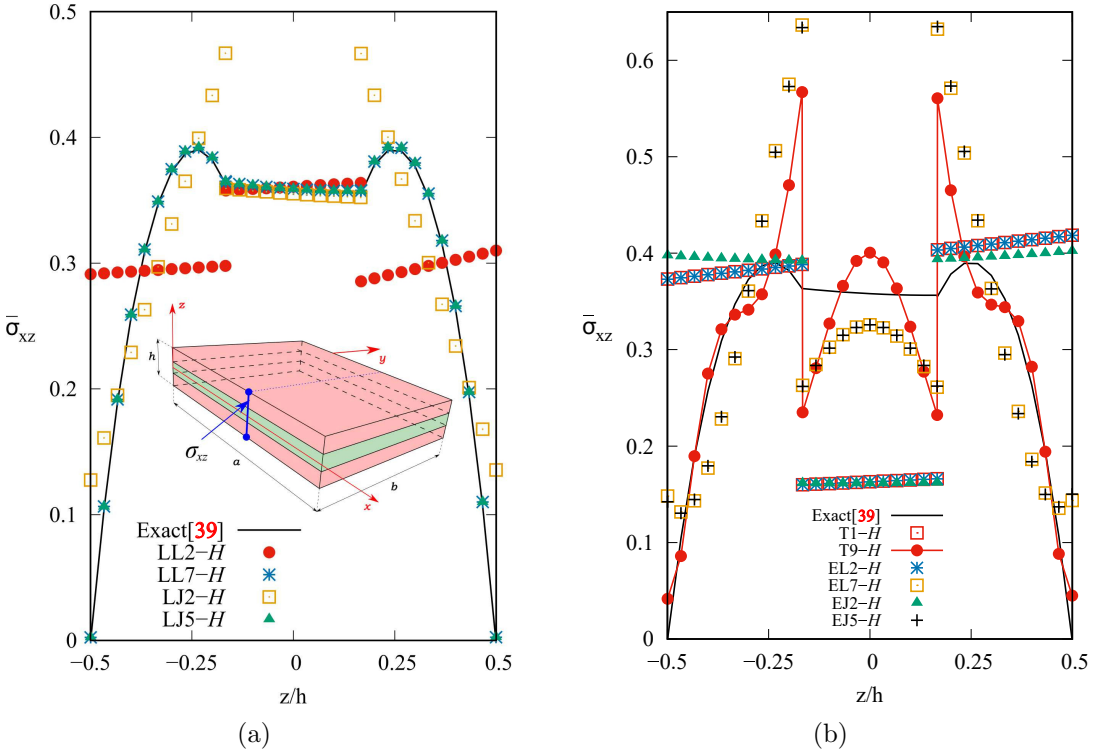

Figure 10: Shear stresses in $[a/2, 0, z]$ for three-layer composite plate loaded by sinusoidal pressure with 2D formulation for $b/h = 4$ case using Hooke's law for LW (a) and ESL (b) approaches.

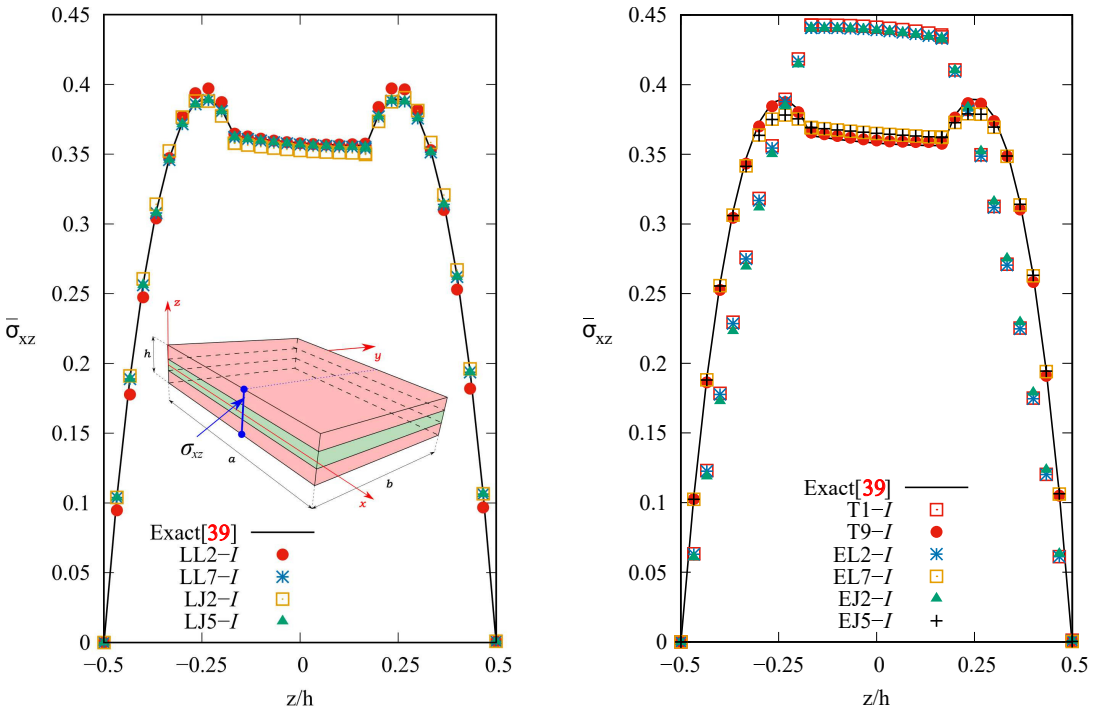

(a) (b)

Figure 11: Shear stresses in $[a/2, 0, z]$ for three-layer composite plate loaded by sinusoidal pressure with 2D formulation for $b/h = 4$ case using stress recovery for LW (a) and ESL (b) approaches.

- Several problems arise by using Hooke's Law for the calculation of the shear stresses. None of the considered ESL models can evaluate the correct distribution. This is due to the anisotropy in the material properties along the transverse direction.
- When adopting the stress recovery method, the LW solutions differ from the reference solution. Higher-order ESL models are similar to the LW ones, while theories with fewer degrees of freedom differ from LW integrated theories and reference solution.
- The use of Taylor, ESL Lagrange and ESL Jacobi leads to similar accuracies.

4.4 Three-layer composite shell

A cylindrical shell is studied as the last benchmark. Thick $R_\beta/h = 4$ and thin $R_\beta/h = 100$ shells were considered. The material properties are the same as the three-layer composite plate example. The reference solution comes from Ren [42]. The results are reported in a non-dimensional form as follows

$$\overline{w} = \frac{10\ E_T\ w}{p_z\ h\ \left(\frac{R_\beta}{h}\right)^4} \qquad \overline{\sigma}_{\beta\beta} = \frac{\sigma_{\beta\beta}}{p_z \left(\frac{R_\beta}{h}\right)^2} \qquad \overline{\sigma}_{\beta z} = \frac{\sigma_{\beta z}}{p_z \left(\frac{R_\beta}{h}\right)} \tag{22}$$

One sub-domain for each layer is used when adopting the LW Lagrange and Jacobi models. The thin shell $R_\beta/h = 100$ is analysed first. Table 8 shows a comparison for several kinematic theories. Transverse displacements, in-plane and shear stresses are shown. The distribution of the shear stresses using Hooke's law is plotted in Fig. 14. On the other hand, Fig. 15

Model	$\overline{u}_z$	$\overline{\sigma}_{xx}$	$\overline{\sigma}_{xz}$		DOF
			H	I	
LW[40]	3.1167	-0.7819	0.1825	—	27783
Taylor and Classical Models					
CLT	2.9363	-0.7697	—	0.0520	22326
FSDT	2.9429	-0.8004	0.0048	0.1692	22326
T1	2.9429	-0.8004	0.0048	0.1692	22326
T3	3.0220	-0.7738	0.0929	0.1768	44652
T5	3.1089	-0.7769	0.2306	0.1774	66978
T7	3.0777	-0.7690	0.2094	0.1774	89304
T9	3.1090	-0.7738	0.1540	0.1775	111630
LW Lagrange					
LL2	3.1241	-0.7780	0.1823	0.1776	44652
LL3	3.1167	-0.7762	0.1859	0.1776	78141
LL4	3.1167	-0.7762	0.1825	0.1776	111630
LL5	3.1167	-0.7762	0.1825	0.1776	145119
LL6	3.1167	-0.7762	0.1825	0.1776	178608
LL7	3.1167	-0.7762	0.1825	0.1776	212097
ESL Lagrange					
EL2	2.8218	-0.7674	0.0048	0.1626	22326
EL3	2.9429	-0.7713	0.0048	0.1620	33489
EL4	3.0222	-0.7739	0.0929	0.1769	44652
EL5	3.0222	-0.7738	0.0929	0.1769	55815
EL6	3.1088	-0.7690	0.2306	0.1775	66978
EL7	3.1088	-0.7699	0.2306	0.1775	78141
LW Jacobi					
LJ1	3.1241	-0.7762	0.1823	0.1776	44652
LJ2	3.1167	-0.7762	0.1859	0.1776	78141
LJ3	3.1167	-0.7762	0.1825	0.1776	111630
LJ4	3.1167	-0.7762	0.1825	0.1776	145119
LJ5	3.1167	-0.7762	0.1825	0.1776	178608
ESL Jacobi					
EJ1	2.8218	-0.7674	0.0048	0.1626	22326
EJ2	2.9429	-0.7713	0.0048	0.1620	33489
EJ3	3.0222	-0.7739	0.0929	0.1769	44652
EJ4	3.0222	-0.7738	0.0929	0.1769	55815
EJ5	3.1088	-0.7690	0.2306	0.1775	66978

Table 7: Transverse displacement, in-plane and shear stresses of the five-layer composite sandwich plate loaded by bi-sinusoidal pressure with 2D formulation. $\overline{u}_z$ calculated in $[a/2, a/2, +h/2]$, $\overline{\sigma}_{xx}$ calculated in $[a/2, a/2, -h/2]$, $\overline{\sigma}_{xz}$ calculated in $[0, a/2, 0]$.

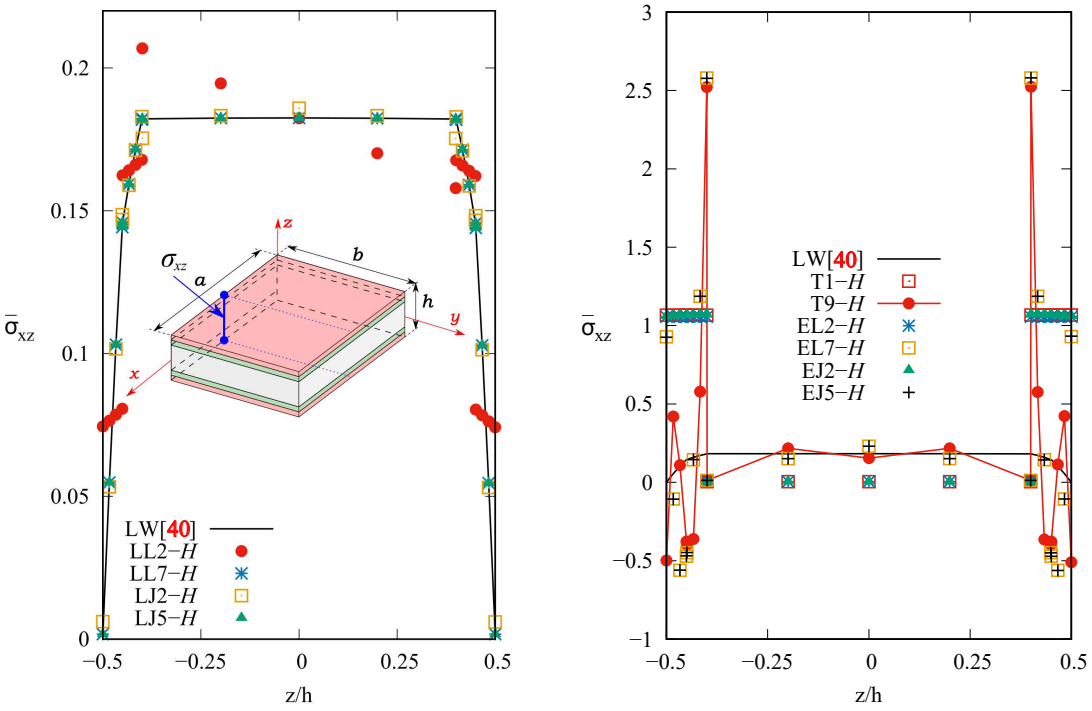

(a) (b)

Figure 12: Shear stress in $[0, a/2, z]$ of five-layer composite sandwich loaded by bi-sinusoidal pressure with 2D formulation using Hooke's law for LW (a) and ESL (b) approaches.

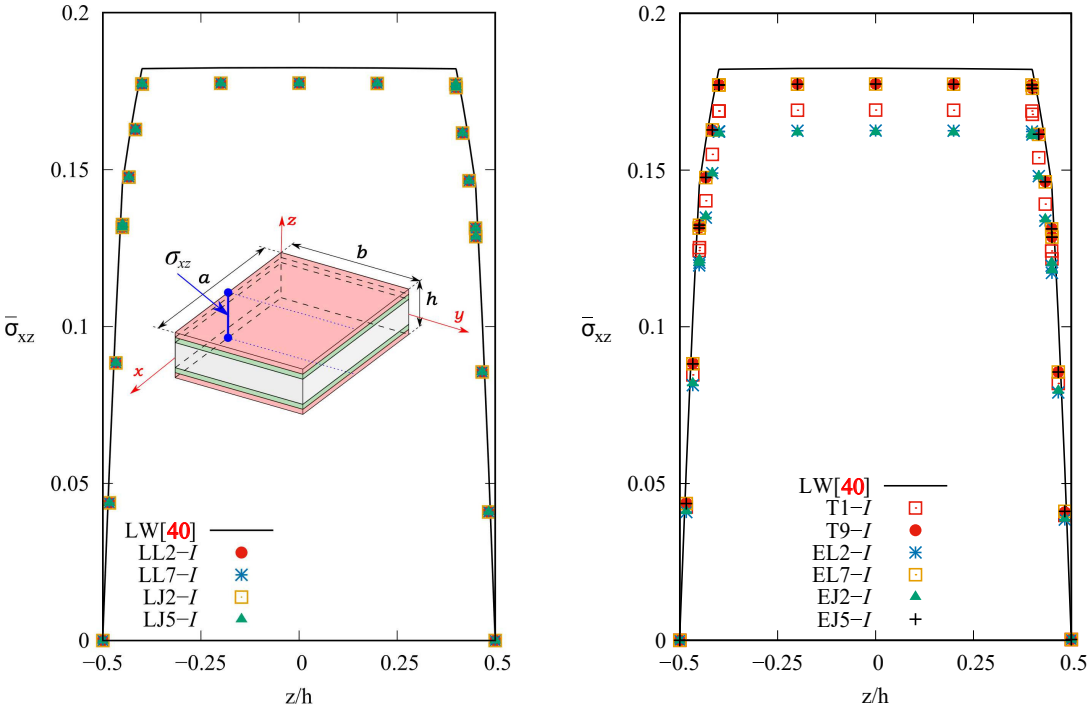

(a) (b)

Figure 13: Shear stress in $[0, a/2, z]$ of five-layer composite sandwich loaded by bi-sinusoidal pressure with 2D formulation using stress recovery for LW (a) and ESL (b) approaches.

illustrates the results obtained through the stress recovery technique.
As far as the thick shell $R_\beta/h = 4$ is considered, Table 8 presents a list of several results for the transverse displacements, in-plane and shear stresses. The distribution of the shear stresses using Hooke's law is given in Fig. 16, while the stress recovery technique is shown in Fig. 17.
The analysis of the shell highlights the following conclusions:

- Higher-order ESL kinematics and LW theories are close to the reference solution when the transverse displacements are evaluated in the thin shell. Classical models and lower-order kinematics are not able to accurately evaluate the solution. Regarding the in-plane stresses, the same considerations can be drawn. Dealing with the transverse displacements and in-plane stresses for the thick shell, lower-order models are not capable of being close to the Exact solution. On the other hand, almost every LW models predict the results very well, except LL2 and LJ1.

- As far as the shear stresses calculated via Hooke's Law are considered for the thin shell, only the LW models almost fit the reference solution distribution. However, lower-order LW theories such as LL2 or LJ2 do not match the reference solutions. As in the previous case, no ESL model cannot reach the exact solution. When the thick plate is considered, only very refined LW theories, i.e. LJ5, are very close to the exact solution.

- If the stress recovery method is employed, it can improve the results for the LW models as for the lower-order theories. In particular, when the thin shell is analysed, every kinematics matches the reference solution. When the thick case is studied, good results are obtained for all the LW models, even for the lower-order LW theories. Furthermore, this method leads to remarkable results also for ESL theories, which can respect the continuity and zero conditions at the top and bottom positions.

- It is confirmed that the same results are obtained if Taylor, ESL Lagrange and Jacobi are adopted. The same considerations is true for Lagrange and Jacobi LW.

5 Conclusions

This paper has evaluated the efficacy of the stress recovery technique for calculating the out-of-plane stress components in the static analysis of composite beams, plates and shells. The Carrera Unified Formulation (CUF) was adopted to build beam, plate and shell models using Equivalent Single-Layer (ESL) and Layer-Wise (LW) approaches. Lower- and higher-order theories were employed based on Taylor, Lagrange and Jacobi polynomials. Four case studies were taken from well-known literature benchmarks, including beam, plate and shell composite structures with various boundary conditions and external loads. The results were compared with those from refined LW models and the literature. The following conclusions can be drawn:

- The stress recovery technique can accurately evaluate the out-of-plane stress components for thin beams, plates and shells regardless of the order of the employed theory of structure. However, this is not valid when cases with transverse anisotropy are considered.

- Hooke's law leads to accurate out-of-plane stresses when LW models are used, i.e., there is no need for the stress recovery technique.

Model	$R_\beta/h = 4$					$R_\beta/h = 100$				
	$\overline{u}_z$	$\overline{\sigma}_{\beta\beta}$	$\overline{\sigma}_{\beta z}$ (H)	$\overline{\sigma}_{\beta z}$ (I)	DOF	$\overline{u}_z$	$\overline{\sigma}_{\beta\beta}$	$\overline{\sigma}_{\beta z}$ (H)	$\overline{\sigma}_{\beta z}$ (I)	DOF
Exact[42]	0.457	1.367	—	0.476	—	0.0787	0.781	—	0.523	—
Taylor and Classical Models										
CLT	0.074	0.654	—	0.490	1314	0.0778	0.776	—	0.414	14418
FSDT	0.293	1.318	0.178	0.496	1314	0.0781	0.776	0.189	0.525	14418
T1	0.331	0.762	0.209	0.583	1314	0.0781	0.776	0.189	0.525	14418
T3	0.425	1.318	0.375	0.508	2628	0.0783	0.777	0.373	0.523	28836
T5	0.435	1.315	0.429	0.489	3942	0.0784	0.777	0.475	0.523	43254
T7	0.445	1.332	0.497	0.483	5256	0.0784	0.777	0.551	0.523	57672
T9	0.448	1.335	0.532	0.482	6570	0.0784	0.777	0.584	0.523	72090
LW Lagrange										
LL2	0.440	1.199	0.478	0.479	2628	0.0783	0.777	0.522	0.523	28836
LL3	0.454	1.334	0.471	0.472	4599	0.0784	0.777	0.522	0.523	50463
LL4	0.458	1.354	0.475	0.477	6570	0.0784	0.777	0.523	0.523	72090
LL5	0.458	1.354	0.475	0.477	8541	0.0784	0.777	0.523	0.523	93717
LL6	0.458	1.354	0.475	0.477	10512	0.0784	0.777	0.523	0.523	115344
LL7	0.458	1.334	0.475	0.477	12483	0.0784	0.777	0.523	0.523	136971
ESL Lagrange										
EL2	0.331	0.759	0.209	0.583	1314	0.0778	0.776	0.189	0.523	14418
EL3	0.329	0.789	0.209	0.584	1971	0.0781	0.776	0.189	0.523	21627
EL4	0.425	1.318	0.375	0.510	2628	0.0783	0.777	0.373	0.523	28836
EL5	0.426	1.306	0.375	0.510	3285	0.0783	0.777	0.373	0.523	36045
EL6	0.435	1.315	0.429	0.490	3942	0.0784	0.777	0.475	0.523	43254
EL7	0.435	1.314	0.429	0.490	4599	0.0784	0.777	0.475	0.523	50463
LW Jacobi										
LJ1	0.440	1.199	0.478	0.479	2628	0.0783	0.777	0.522	0.523	28836
LJ2	0.454	1.334	0.471	0.472	4599	0.0784	0.777	0.522	0.523	50463
LJ3	0.458	1.354	0.475	0.477	6570	0.0784	0.777	0.523	0.523	72090
LJ4	0.458	1.354	0.475	0.477	8541	0.0784	0.777	0.523	0.523	93717
LJ5	0.458	1.354	0.475	0.477	10512	0.0784	0.777	0.523	0.523	115344
ESL Jacobi										
EJ1	0.331	0.759	0.209	0.583	1314	0.0778	0.776	0.189	0.523	14418
EJ2	0.329	0.789	0.208	0.584	1971	0.0781	0.776	0.189	0.523	21627
EJ3	0.425	1.318	0.375	0.510	2628	0.0783	0.777	0.373	0.523	28836
EJ4	0.426	1.306	0.375	0.510	3285	0.0783	0.777	0.373	0.523	36045
EJ5	0.435	1.315	0.429	0.490	3942	0.0784	0.777	0.475	0.523	43254

Table 8: Transverse displacement, in-plane and shear stresses of three-layer composite shell loaded by sinusoidal pressure with 2D shell formulation. $\overline{u}_z$ calculated in $[a/2, b/2, 0]$, $\overline{\sigma}_{\beta\beta}$ calculated in $[a/2, b/2, h/2]$ and $\overline{\sigma}_{\beta z}$ calculated in $[a/2, 0, 0]$.

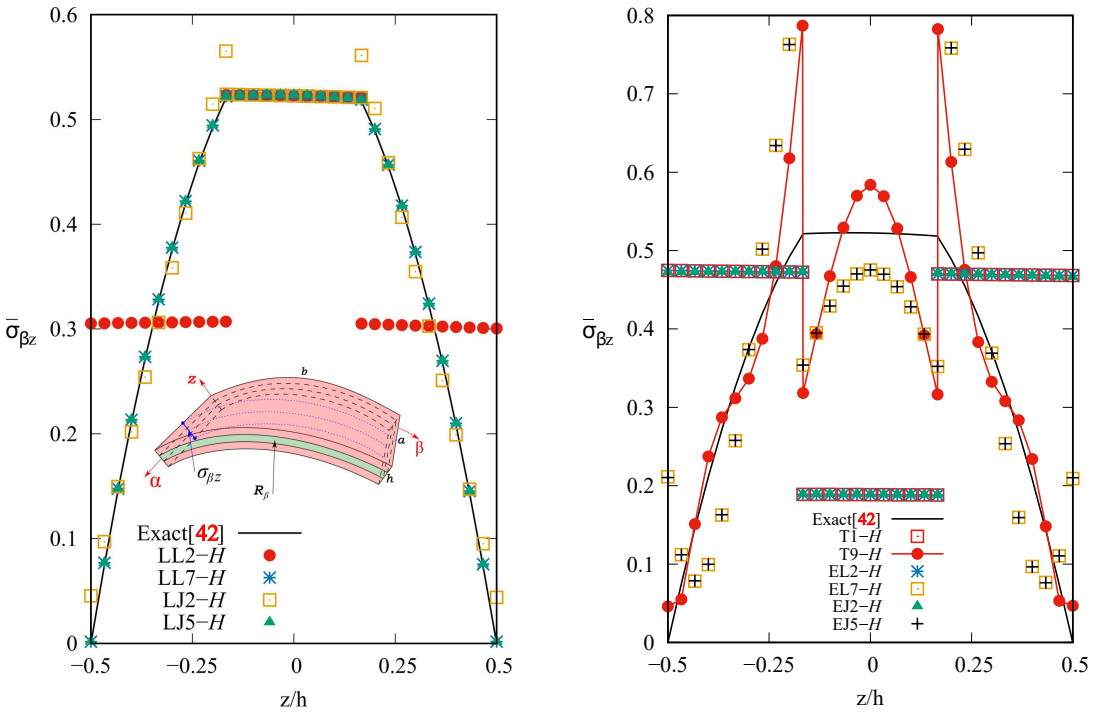

Figure 14: Shear stresses in $[a/2, 02, z]$ for three-layer composite shell loaded by sinusoidal pressure with 2D shell formulation for $R_\beta/b = 100$ case using Hooke's law

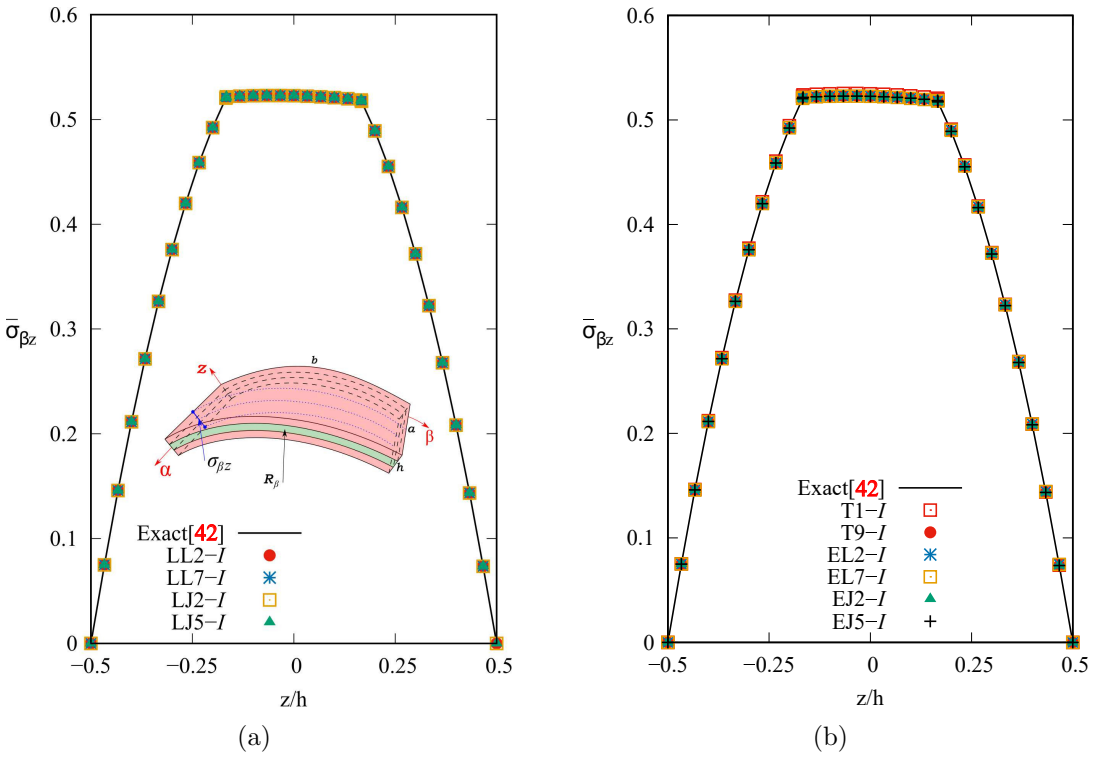

Figure 15: Shear stresses in $[a/2, 0, z]$ for three-layer composite shell loaded by sinusoidal pressure with 2D shell formulation for $R_\beta/b = 100$ case using stress recovery for LW (a) and ESL (b) approaches.

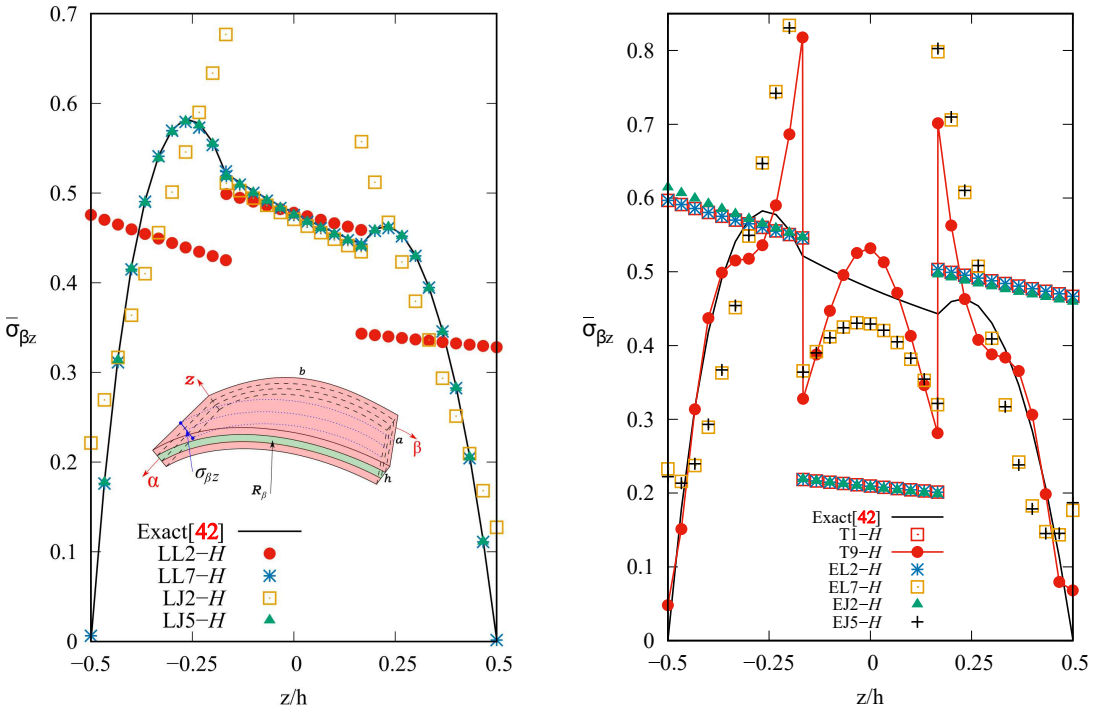

Figure 16: Shear stresses in $[a/2, 0, z]$ for three-layer composite shell loaded by sinusoidal pressure with 2D shell formulation for $R_\beta/b = 4$ case using Hooke's law for LW (a) and ESL (b) approaches.

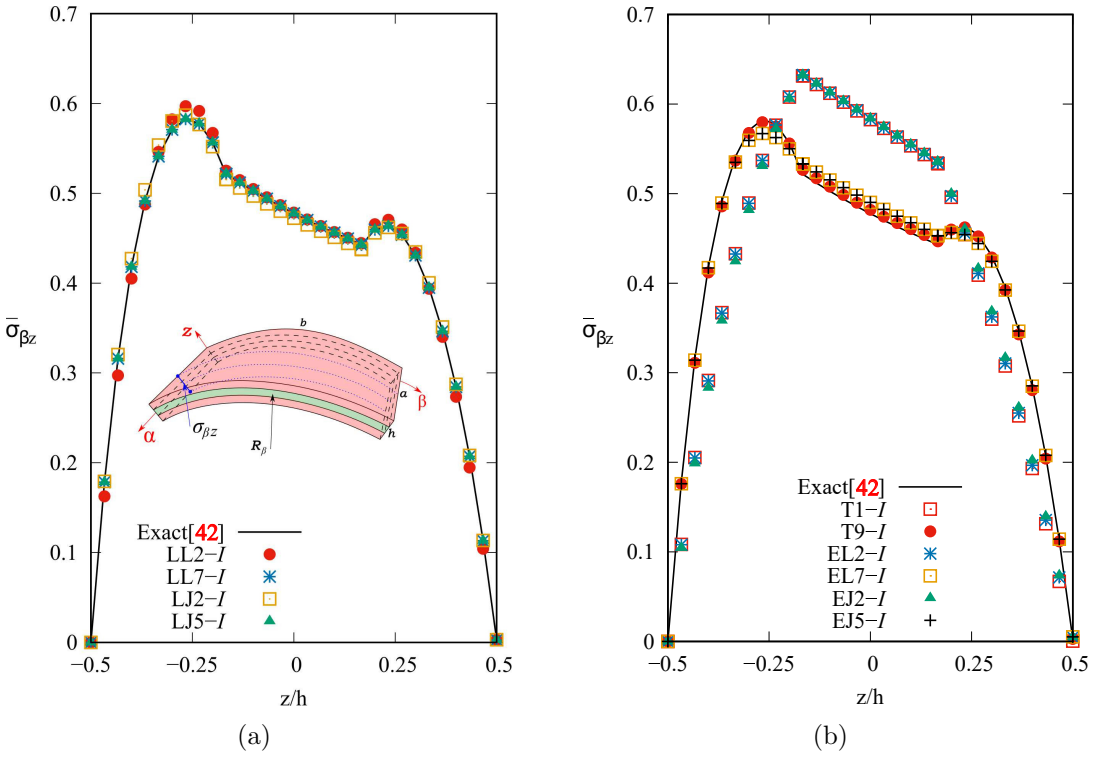

Figure 17: Shear stresses in $[a/2, 0, z]$ for three-layer composite shell loaded by sinusoidal pressure with 2D shell formulation for $R_\beta/b = 4$ case using stress recovery for LW (a) and ESL (b) approaches.

- When dealing with thick structures, the stress recovery technique can improve the accuracy of ESL models, but the results are still not as accurate as those from refined LW models.

References

[1] L. Euler. *Methodus inveniendi lineas curvas maximi minimive proprietate gaudentes sive solutio problematis isoperimetrici latissimo sensu accepti*, volume 1. Springer Science & Business Media, Berlin, Germany, 1952.

[2] G. Kirchhoff. Über das gleichgewicht und die bewegung einer elastischen scheibe. *Journal für die reine und angewandte Mathematik (Crelles Journal)*, 1850(40):51–88, 1850.

[3] A.E.H. Love. *A treatise on the mathematical theory of elasticity*. Cambridge University Press, 1927.

[4] E. Reissner and Y. Stavsky. Bending and stretching of certain types of heterogeneous aeolotropic elastic plates. *Journal of Applied Mechanics*, 28:402–408, 1961.

[5] S.P. Timoshenko. On the transverse vibrations of bars of uniform cross section. *Philosophical Magazine*, 43:125–131, 1922.

[6] E. Reissner. The effect of transverse shear deformation on the bending of elastic plates. *Journal of Applied Mechanics*, 12:69–77, 1945.

[7] R. Mindlin. Influence of rotary inertia and shear flexural motion of isotropic, elastic plates. *Journal of Applied Mechanics*, 18:31–38, 1951.

[8] E. Carrera. Evaluation of layerwise mixed theories for laminated plates analysis. *AIAA journal*, 36(5):830–839, 1998.

[9] V.V. Novozhilov. *Theory of elasticity*. Pergamon, Elmsford, 1961.

[10] R.K. Kapania and S. Raciti. Recent advances in analysis of laminated beams and plates. Part I: Shear effects and buckling. *AIAA journal*, 27(7):923–935, 1989.

[11] R.K. Kapania and S. Raciti. Recent advances in analysis of laminated beams and plates. Part II: Vibrations and wave propagation. *AIAA journal*, 27(7):935–946, 1989.

[12] E. Carrera, A. Pagani, M. Petrolo, and E. Zappino. Recent developments on refined theories for beams with applications. *Mechanical Engineering Reviews*, 2(2):14–00298–14–00298, 2015.

[13] V.Z. Vlasov. *Thin-walled elastic beams*. National Technical Information Service, 1984.

[14] R.D. Ambrosini, J. D. Riera, and R. F. Danesi. A modified Vlasov theory for dynamic analysis of thin-walled and variable open section beams. *Engineering Structures*, 22(8):890–900, 2000.

[15] I. Mechab, N. El Meiche, and F. Bernard. Analytical study for the development of a new warping function for high order beam theory. *Composites Part B: Engineering*, 119:18–31, 2017.

[16] P.O. Friberg. Beam element matrices derived from Vlasov's theory of open thin-walled elastic beams. *International Journal for Numerical Methods in Engineering*, 21(7):1205–1228, 1985.

[17] M. Ganapathi, B. P. Patel, O. Polit, and M. Touratier. A c1 finite element including transverse shear and torsion warping for rectangular sandwich beams. *International Journal for Numerical Methods in Engineering*, 45(1):47–75.

[18] P. Vidal and O. Polit. A family of sinus finite elements for the analysis of rectangular laminated beams. *Composite Structures*, 84:56–72, 06 2008.

[19] R. Schardt. Eeine erweiterung der technischen biegetheorie zur berechnung prismatischer faltwerke. *Der Stahlbau*, 35:161–171, 1966.

[20] W. Yu, V.V. Volovoi, D.H. Hodges, and X. Hong. Validation of the Variational Asymptotic Beam Sectional analysis. *AIAA Journal*, 40(10):2105–2112, 2002.

[21] J.N. Reddy and D. H. Robbins Jr. Theories and Computational Models for Composite Laminates. *Applied Mechanics Reviews*, 47(6):147–169, 06 1994.

[22] E. Carrera. Developments, ideas, and evaluations based upon reissner's mixed variational theorem in the modeling of multilayered plates and shells. *Appl. Mech. Rev.*, 54(4):301–329, 2001.

[23] J.N. Reddy. A Simple Higher-Order Theory for Laminated Composite Plates. *Journal of Applied Mechanics*, 51(4):745–752, 12 1984.

[24] H. Murakami. Laminated composite plate theory with improved in-plane responses. *Journal of Applied Mechanics*, 53(3):661–666, 09 1986.

[25] E. Carrera. Theories and finite elements for multilayered plates and shells: a unified compact formulation with numerical assessment and benchmarking. *Archives of Computational Methods in Engineering*, 10(3):215–296, 2003.

[26] F.G. Rammerstorfer, K. Dorninger, and A. Starlinger. Composite and sandwich shells. In *Nonlinear analysis of shells by finite elements*, pages 131–194. Springer, 1992.

[27] J.N. Reddy. An evaluation of equivalent-single-layer and layerwise theories of composite laminates. *Composite structures*, 25(1-4):21–35, 1993.

[28] A.S. Mawenya and J.D. Davies. Finite element bending analysis of multilayer plates. *International Journal for Numerical Methods in Engineering*, 8(2):215–225, 1974.

[29] A.K. Noor and W.S. Burton. Assessment of computational models for multilayered composite shells. *Applied Mechanics Reviews*, 43:67–97, 1990.

[30] E. Carrera. A priori vs. a posteriori evaluation of transverse stresses in multilayered orthotropic plates. *Composite Structures*, 48(4):245–260, 2000.

[31] M. Patni, S. Minera, R.M.J. Groh, A. Pirrera, and P.M. Weaver. Three-dimensional stress analysis for laminated composite and sandwich structures. *Composites Part B: Engineering*, 155:299–328, 2018.

[32] B.C Park, J.W. Park, and Y.H Kim. Stress recovery in laminated composite and sandwich panels undergoing finite rotation. *Composite Structures*, 59(2):227–235, 2003.

[33] E. Carrera, A. Pagani, and S. Valvano. Shell elements with through-the-thickness variable kinematics for the analysis of laminated composite and sandwich structures. *Composites Part B: Engineering*, 111:294–314, 2017.

[34] E. Carrera, M. Cinefra, E. Zappino, and M. Petrolo. *Finite Element Analysis of Structures Through Unified Formulation*. Prentice hall, John Wiley & Sons Ltd, 2014.

[35] K.J. Bathe. *Finite Element Procedure*. Prentice hall, Upper Saddle River, New Jersey, USA, 1996.

[36] T.J.R. Hughes. *The Finite Element Method: Linear Static and Dynamic Finite Element Analysis*. Courier Corporation, 2012.

[37] E. Carrera, G. Giunta, and M. Petrolo. *Beam structures: classical and advanced theories*. John Wiley & Sons, 2011.

[38] E. Carrera, R. Augello, and D. Scano. Use of ESL lagrange theories for beams, plates and shells. *Atti dell'Accademia delle Scienze*, 2022.

[39] N.J. Pagano. Exact solutions for composite laminates in cylindrical bending. *Journal of Composite Materials*, 3(3):398–411, 1969.

[40] A. Pagani, S. Valvano, and E. Carrera. Analysis of laminated composites and sandwich structures by variable-kinematic MITC9 plate elements. *Journal of Sandwich Structures & Materials*, 20(1):4–41, 2018.

[41] M. Petrolo and A. Lamberti. Axiomatic/asymptotic analysis of refined layer-wise theories for composite and sandwich plates. *Mechanics of Advanced Materials and Structures*, 23(1):28–42, 2016.

[42] J.G. Ren. Exact solutions for laminated cylindrical shells in cylindrical bending. *Composites Science and Technology*, 29(3):169–187, 1987.

[43] E. Carrera, M. Cinefra, M. Petrolo, and E. Zappino. *Finite element analysis of structures through unified formulation*. John Wiley & Sons, 2014.

[44] M. Abramowitz and I. A. Stegun. *Handbook of Mathematical Functions with Formulas, Graphs, and Mathematical Tables*. Dover Pubblications, 1964.

[45] E. Carrera, M. Cinefra, and G. Li. Refined finite element solutions for anisotropic laminated plates. *Composite Structures*, 183:63–76, 2018. In honor of Prof. Y. Narita.

A Structural theories for beams, plates and shells

In this paper, Taylor, Lagrange and Jacobi polynomials are used as expansion functions for the evaluation of the displacements over the cross-section (1D beams) and thickness (2D plates and shells) of composite structures.

Taylor polynomials For the 2D plate and shell formulations, one-dimensional functions depend only on the thickness coordinate z and they can be generally written as follows:

$$F_0 = z = 1, \quad F_1 = z^1 = z, \ldots, F_N = z^N \tag{23}$$

In a 1D beam formulation, 2D polynomials $x^i z^j$ are used (i and j are positive integers). An example of a second-order displacement field is

$$\begin{aligned} u_x &= u_{x_1} + x u_{x_2} + z u_{x_3} + x^2 u_{x_4} + xz u_{x_5} + z^2 u_{x_6} \\ u_y &= u_{y_1} + x u_{y_2} + z u_{y_3} + x^2 u_{y_4} + xz u_{y_5} + z^2 u_{y_6} \\ u_z &= u_{z_1} + x u_{z_2} + z u_{z_3} + x^2 u_{z_4} + xz u_{z_5} + z^2 u_{z_6} \end{aligned} \tag{24}$$

It is possible to obtain classical theories for both formulations by imposing $N = 1$ and using penalty techniques, see [43].

Lagrange polynomials The general formula for 1D Lagrange polynomials is written as

$$F_m(\zeta) = \prod_{l=0, j\neq m}^{n} \frac{\zeta - \zeta_l}{\zeta_m - \zeta_l} = \frac{(\zeta - \zeta_0)\ldots(\zeta - \zeta_{m-1})\ldots(\zeta - \zeta_n)}{(\zeta_m - \zeta_0)\ldots(\zeta_m - \zeta_{m-1})(\zeta_m - \zeta_{m+1})\ldots(\zeta_m - \zeta_n)} \tag{25}$$

where ζ is the natural coordinate $[-1, +1]$, m is the actual coordinate, n denotes the number of the $l - th$ roots (namely, the Lagrange Points, LPs) of the polynomial. The polynomial order of the expansion is equal to $n - 1$. The domain in the natural coordinate is [-1,+1]. For 2D plate and shell formulations, six different one-dimensional interpolations are adopted: 2 LPs, 3 LPs, 4 LPs, 5 LPs, 6 LPs, 7 LPs.
The 1D beam formulation uses bi-dimensional functions for the cross-section approximation. In this work, three kinds of interpolations are used: bi-linear interpolation is given by 4LPs, bi-quadratic interpolation is created by 9LPs and bi-cubic interpolation by 16LPs. More details can be found in [43].

Jacobi polynomials The orthogonal Jacobi polynomials are built by using a recurrence relation,

$$P_n^{(\gamma,\theta)}(\zeta) = (A_n \zeta + B_n)\, P_{n-1}^{(\gamma,\theta)}(\zeta) - C_n P_{n-2}^{(\gamma,\theta)}(\zeta) \tag{26}$$

where γ and θ are two parameters and n is the polynomial order. The relation is calculated in $\zeta = [-1, +1]$, with $P_0^{(\gamma,\theta)}(\zeta) = 1$ and $P_1^{(\gamma,\theta)}(\zeta) = A_0\zeta + B_0$. The parameters A_n, B_n and C_n are given in Abramowitz and Stegun [44]. Other popular polynomials can be devised by opportunely choosing values of the parameters γ and θ. For instance, Legendre polynomials are given by $\gamma = 0$ and $\theta = 0$. For 2D plate and shell formulation, one-dimensional expansions can be derived by adopting the Jacobi polynomials and the following expressions

$$\begin{aligned} F_1(\zeta) &= \frac{1}{2}(1 - \zeta) \\ F_2(\zeta) &= \frac{1}{2}(1 + \zeta) \\ F_\tau(\zeta) &= \phi_{\tau-1}(\zeta), \quad \tau = 3, 4, ..., n + 1 \end{aligned} \tag{27}$$

with

$$\phi_j(\zeta) = (1 - \zeta)(1 + \zeta) P_{j-2}^{\gamma,\theta}(\zeta), \quad j = 2, 3, ..., n \tag{28}$$

The first two functions $F_1(\zeta)$, $F_2(\zeta)$ are the vertex expansions. Given the following property,

$$F_\tau(-1) = F_\tau(1) = 0, \quad i \geq 3 \tag{29}$$

the functions $F_\tau(\zeta), \tau = 3, 4, ...$ are called bubble functions or edge expansions. Jacobi polynomials are also adopted to build two-dimensional expansions for 1D formulation. In this case, vertex, edge and internal polynomials are used as interpolation functions over the domain, see [45] for more details. The vertex modes correspond to the first-order, quadrilateral Lagrange polynomials:

$$F_\tau(\xi, \eta) = \frac{1}{4}(1 - \xi_\tau \xi)(1 - \eta_\tau \eta), \quad \tau = 1, 2, 3, 4 \tag{30}$$

where ξ and η vary above the domain between -1 and +1, and ξ_τ and η_τ represent the vertex coordinates in the natural plane. The edge modes are defined for $p \geq 2$ as follows

$$\begin{aligned}
F_\tau(\xi, \eta) =& \frac{1}{2}(1 - \eta)\,\phi_p(\xi), \quad \tau = 5, 9, 13, 18, ... \\
F_\tau(\xi, \eta) =& \frac{1}{2}(1 + \xi)\,\phi_p(\eta), \quad \tau = 6, 10, 14, 19, ... \\
F_\tau(\xi, \eta) =& \frac{1}{2}(1 + \eta)\,\phi_p(\xi), \quad \tau = 7, 11, 15, 20, ... \\
F_\tau(\xi, \eta) =& \frac{1}{2}(1 - \xi)\,\phi_p(\eta), \quad \tau = 8, 12, 16, 21, ...
\end{aligned} \tag{31}$$

where p represents the polynomial degree of the bubble function. The internal expansions are built by multiplying edge modes defined for one-dimensional equations, given for $p \geq 4$. The number of internal polynomials is provided by $(p-2)(p-3)/2$. The set of fifth-order polynomials, which contains 3 internal expansions, is shown as an example

$$\begin{aligned}
F_{22}(\xi, \eta) =& \phi_3(\xi)\phi_2(\eta), \quad 3 + 2 = 5 \\
F_{23}(\xi, \eta) =& \phi_2(\xi)\phi_3(\eta), \quad 2 + 3 = 5 \\
F_{17}(\xi, \eta) =& \phi_2(\xi)\phi_2(\eta), \quad 2 + 2 = 4
\end{aligned} \tag{32}$$

In this work, ESL models that make use of Taylor, Lagrange and Jacobi polynomials are used. The general behaviour of the primary mechanical variables along the thickness of the structure in the case of ESL is depicted in Fig. 18 for a three-layer plate. In the case of LW,

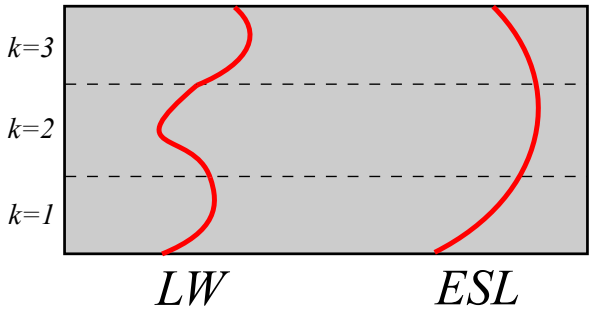

Figure 18: Scheme for modelling approaches. k is the index of the layers.

different sets of variables are assumed per each layer and the continuity of the displacements is imposed at the layer interface (see Fig. 18), and is obtained using Lagrange and Jacobi polynomials.